Aerosol and Air Quality Research, 16: 2635–2654, 2016

ISSN: 1680-8584 print / 2071-1409 online
doi: 10.4209/aaqr.2015.07.0463

Impact of Smoke Intensity on Size-Resolved Aerosol Composition and Microstructure during the Biomass Burning Season in Northwest Vietnam

Olga B. Popovicheva[1*], Guenter Engling[2,3], Evangelia Diapouli[4], Dikaia Saraga[4], Natalia M. Persiantseva[1], Mikhail A. Timofeev[1], Elena D. Kireeva[1], Natalia K. Shonija[1], Sheng-Han Chen[2], Dac L. Nguyen[5], Konstantinos Eleftheriadis[4], Chung-Te Lee[6]

[1] *Skobeltsyn Institute of Nuclear Physics, Lomonosov Moscow State University, Moscow1 19991, Russia*
[2] *Department of Biomedical Engineering and Environmental Sciences, National Tsing Hua University, Hsinchu 30013, Taiwan*
[3] *Division of Atmospheric Sciences, Desert Research Institute, Reno, NV 89512, USA*
[4] *Institute of Nuclear & Radiological Sciences & Technology, Energy & Safety, N.C.S.R. "Demokritos", Athens 15310, Greece*
[5] *Institute of Geophysics - Vietnam Academy of Science and Technology, Ha Noi, Vietnam*
[6] *Graduate Institute of Environmental Engineering, National Central University, Chung-Li 32001, Taiwan*

ABSTRACT

Aerosol particles significantly impact the regional environment, including climate change, specifically in periods of extensive biomass burning. The major agricultural and domestic combustion emission sources were assessed in near-source and ambient monitoring campaigns in northwestern Vietnam during the dry season. The composition and microstructure of on-field burning and cooking emissions were analyzed with a variety of techniques. A wide range of observed $PM_{2.5}$ mass concentrations was categorized according to the smoke level, supported by the evolution of carbon fractions (OC and EC) as well as ionic species and molecular tracers (K^+, levoglucosan, and mannosan). The OC/EC and individual organic compound ratios on days with high smoke levels indicate smoldering combustion of softwood and other local biomass species, impacting aerosol composition at the regional level. Acid and non-acid carbonyls, carboxylates, and aliphatic carbon functionalities in the $PM_{2.5}$ size fraction evolved with increasing smoke intensity, together with carbonates in coarse ($PM_{1–2.5}$ and $PM_{2.5–10}$) size fractions, indicating a large impact of smoke emissions and soil lifted up by the intense fires. Biomass burning influence increased the abundance of soot and organic particles in the submicron fraction from 12% at low to 59% and 68% at moderate and high smoke levels, respectively. Smoke micromarkers of local biomass burning source emissions determined the microstructure of ambient aerosols representative for northern Southeast Asia.

Keywords: Biomass combustion; Smoke emission; Near-source sampling; Size segregation; Chemical composition; Morphology.

INTRODUCTION

Vast amounts of air pollution are produced worldwide by burning of billions of tons of biomass, contributing 42% to the global combustion emissions inventory (Bond *et al.*, 2013). Biomass burning (BB) is increasingly recognized as an important source of multicomponent aerosols. Their physico-chemical properties and cloud-forming potential induce harmful effects on the environment, directly and indirectly impacting the Earth's radiation balance, and subsequently affecting regional and global climate. Light-absorbing smoke particles warm the upper layer of the troposphere, reducing surface water evaporation and decreasing the convection that is an essential part of the hydrological cycle (Ramanathan *et al.*, 2001). Emissions and properties of BB aerosols are highly source-dependent, and vary considerably between urban and rural regions, depending on burning practice, combustion phase (open flaming vs. smoldering), and type of biomass. Therefore, quantification of BB emissions is in the focus of current research and abatement strategies, especially given that large regional smoke emissions are a result of numerous fires, and the impacts of BB on regional air quality remain rather uncertain.

BB activities in northern Southeast (SE) Asia peak in

* Corresponding author.
E-mail address: polga@mics.msu.su

February–April and the resulting smoke contributions are comparable to those from anthropogenic emissions (Liu *et al.*, 2003). Monthly-mean values of total carbon emissions during the dry season approach 150 TgC (Tsay *et al.*, 2013). In South Asia, BB contributes to two-thirds of total organic carbon (OC) and about half of elemental carbon (EC) (Gustafsson *et al.*, 2009). In Vietnam, deforestation remains a crucial problem, and agricultural activities include crop (e.g., cassava and corn) and sugar cane pre-harvest burning. Traditional biomass, especially wood, is the dominant energy source for most rural households due to low cost and easy accessibility. Cooking and garbage burning, such as of household waste and garden leaves, are common as well.

Numerous studies have investigated BB impacts on ambient aerosol mass and composition (e.g., Reid *et al.*, 2005; Jaffe *et al.*, 2008; Engling *et al.*, 2011; Chuang *et al.*, 2013). Distinct regional characteristics in BB smoke have been observed, suggesting that local emissions dominate aerosol chemistry (Lim *et al.*, 2012; Tao *et al.*, 2013), while transport and mixing of BB aerosol from upwind sources is commonly observed as well (e.g., Zhang *et al.*, 2012). OC and EC were found to be the main components comprising the aerosol mass during BB events (Amiridis *et al.*, 2012; Popovicheva *et al.*, 2014a). Characterization of organic compounds in ambient aerosols has revealed the extent to which different sources impact particulate matter (PM) concentrations (Coury and Dillner, 2009). Major organic components of BB smoke were found to be monosaccharide derivatives (anhydrosugars) from the thermal breakdown of cellulose, accompanied by aliphatic and oxygenated compounds (Simoneit *et al.*, 1999). Molecular tracers such as levoglucosan and potassium ions confirm the impact of BB activities on ambient aerosol (Engling *et al.*, 2014; Ho *et al.*, 2014). Aside from the carbonaceous components, up to 17% of smoke PM mass may be of mineral origin, dominated by alkali, alkali earth, chlorides and sulfates (Reid *et al.*, 2005; Samsonov *et al.*, 2012). Aging processes, as typically occurring during long-range transport, may significantly change the composition of smoke aerosol at down-wind receptor sites (Posfai *et al.*, 2003; Diapouli *et al.*, 2014).

Knowledge of the chemical composition of size-segregated ambient aerosol is essential to assess aerosol impacts on climate (Ramanathan *et al.*, 2001). Submicron carbonaceous aerosols are of particular concern in respect to environmental change and public health, because they mainly originate from anthropogenic and wildfire sources, and may interact effectively with sunlight (Andrews *et al.*, 2000; Lim *et al.*, 2012). Size-resolved BB chemical composition analysis has demonstrated that the molecular tracers peak in the fine mode of ambient aerosols (Chen *et al.*, 2014; Zhang *et al.*, 2015). Measurements of PM emissions from ten biomass fires showed that potassium ions, chlorides, and sulfates are the dominant inorganic species in the fine mode, while calcium ions are an important component in coarse particles (Park *et al.*, 2013).

High heterogeneity in the aerosol composition observed at microscopic level requires individual particle characterization with respect to morphology and elemental composition (Posfai *et al.*, 2003; Niemi *et al.*, 2006). Seventeen particle types were distinguished in ambient air affected by different combustion sources in the study by Xie *et al.* (2005). Using cluster analyses, several K and Cl-containing groups were found with high abundance in particles from flaming fires, whereas mineral, Si-rich, and light-element particle groups were predominant in the smoke released during the smoldering phase (Liu *et al.*, 2000). A higher abundance of soot agglomerates was observed in flaming fires, while organic particles dominated in smoldering phase emissions, demonstrating a strong dependence of smoke microstructure on combustion temperature (Popovicheva *et al.*, 2015). During an extreme BB event, ambient carbonaceous particles and fly ash exhibited the microstructure of smoke in good agreement with elevated OC and EC fractions (Popovicheva *et al.*, 2014a). BB aerosol released during these wildfires, which was subject to long-range transport, was found to be enhanced in dust groups, comprised of calcium sulfates and carbonates, due to soil entrainment during such intensive fires (Diapouli *et al.*, 2014).

Initiated in 2007, the Seven South-East Asian Studies (7-SEAS) campaign included the Biomass-Burning Aerosols in SE Asia: Smoke Impact Assessment (BASE-ASIA) study (Lin *et al.*, 2013) and seeks to perform interdisciplinary research in the field of aerosol-environment and climate interactions in SE Asia, particularly focusing on the impact of BB on cloud processes, atmospheric radiation, and regional climate (Huang *et al.*, 2013; Tsay *et al.*, 2013). One of the main goals of the 7-SEAS campaign is to characterize the chemical, physical, and optical properties of BB aerosols produced by extensive anthropogenic activities in SE Asia.

This paper reports results from measurements during the 2013 BASE-ASIA campaign with focus on physico-chemical properties of aerosols in the dry season in Son La Province, northwest Vietnam, affected by biomass burning activities, including agricultural and domestic combustion sources. We specifically conducted the characterization of near-source emissions from traditional burning activities (on-field burning and domestic cooking) in order to identify the bulk components comprising the resulting smoke aerosol and major groups in the smoke microstructure. We relate the characteristics of size-segregated aerosol to the ambient aerosol loadings, classified as low, moderate, and high smoke levels, with respect to the evolution of aerosol chemistry and microstructure from the BB emission sources into the ambient atmosphere.

EXPERIMENTAL

Measurement Campaign

The measurement campaign was conducted at a meteorological observation station in Son La Province, northwestern Vietnam (21.33°N, 103.9°E) during 24 February–8 April, 2013. The station was located on a hill at 675 m above sea level (a.s.l.) in the outskirts of Son La city. A MetOne BAM Continuous Particle Monitor in NASA's SMART-COMMIT mobile laboratory was used for measurements of $PM_{2.5}$ mass concentration (http://smartlabs.gsfc.nasa.gov; Tsay *et al.*, 2013). Assuming that the measured PM level may be substantially impacted by BB

activities we ascribe the $PM_{2.5}$ mass concentrations ≤ 40 μg m^{-3} to low smoke intensity, while moderate smoke is in the range from 40 to 80 μg m^{-3} and in the high smoke periods $PM_{2.5}$ was found to be higher than 80 μg m^{-3}. Size-segregated aerosol particles were collected using a 3-stage cascade impactor (PM_{10}, Dekati Ltd.) with a flow rate of 30 L min^{-1}, providing three size fractions. Coarse particles (2.5–10 μm and 1–2.5 μm aerodynamic equivalent diameter) were collected on two separate impaction substrates, 25 mm in diameter, while fine particles (< 1 μm, PM_1), were collected on 47 mm filters at the bottom of the impactor. For microscopic and FTIR analyses, Cu foil was used as impaction substrate, covered by a thin layer of oil (oleic acid) to reduce particle bounce. FTIR spectra of oiled substrates were measured before sampling for quantification of oiling impact on sample chemistry. To assess the effect of the oil coating on quantitative particle composition measurement, on selected days with similar PM mass concentrations oil was not used. In this case, the particle size was assessed by SEM/EDX analysis, in order to be able to compare particles in the size range according to the cutoff diameter of a given impaction stage. For microscopic analyses, samples were collected for approximately one hour, resulting in visible spots on the foil substrates which represented loadings suitable for direct measurements under an electron beam. For FTIR analyses, the samples were collected for about 24 hours. Quartz fiber filters (Tissuquartz 2500 QAT-UP, PALL Corp.) were used as substrates in the Dekati cascade impactor for subsequent chemical analyses. Dekati impaction stages for the 2.5 and 1 μm cut offs have an adequate jet to plate distance to allow close to nominal impaction characteristics even for quartz fiber filters which, due to their thickness in other cases, have been found unsuitable as impaction substrates. In addition, particles equal to or less than 2.5 μm in diameter ($PM_{2.5}$) were collected on quartz fiber and Teflon membrane filters (Teflo, PALL Corp.) by a MiniVol sampler (Airmetrics) at a flow rate of 5 L min^{-1}. To investigate the time dependence of smoke properties, on selected days $PM_{2.5}$ samples were collected for 12 hours, reflecting day and night time.

Numerous fires on agricultural fields, gardens, houses, and small cooking places were observed around the station during the entire measurement campaign, as shown Fig. 1(a). For source emissions characterization, the major types of BB in Son La Province were identified. The most common agricultural practice was cutting off the crowns of forests on the surrounding hills and subsequent burning of the fallen trees, followed by sowing of rice or corn on the fields covered by ash. Another common practice was the burning of piled crop residues, with the motivation to return the

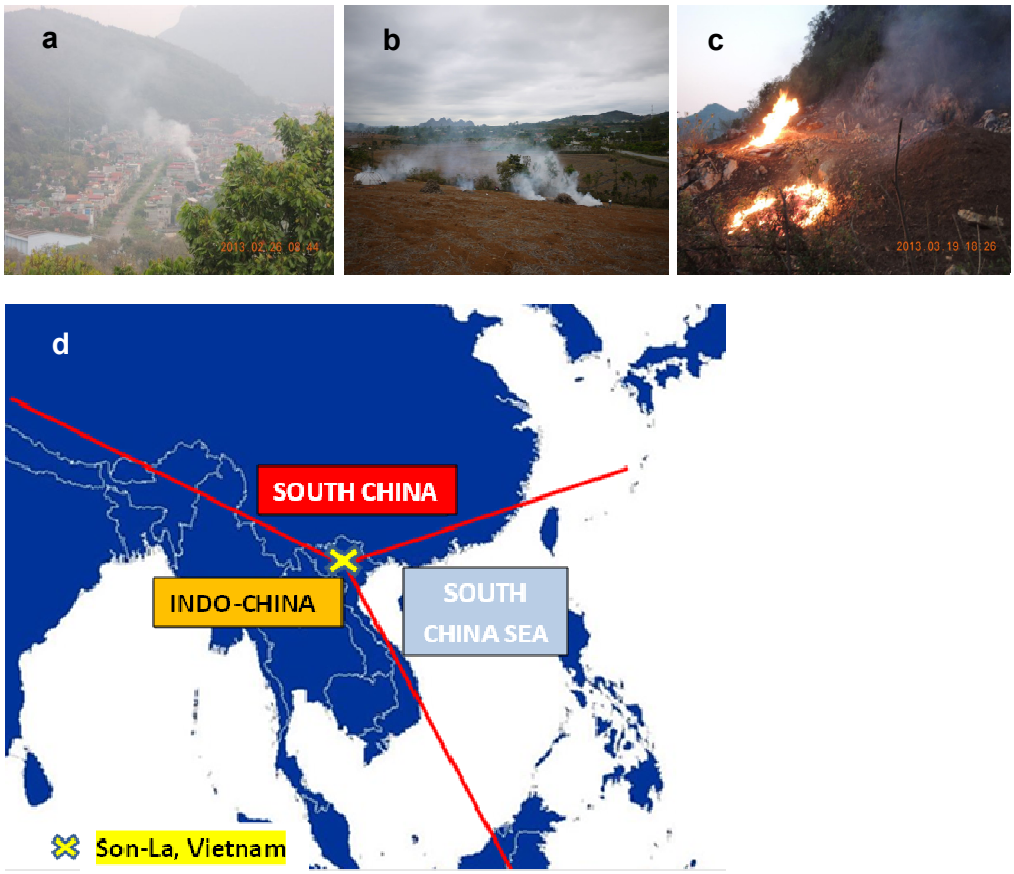

Fig. 1. a) Images of surroundings of the Son La weather/measurement station. Major BB sources in Son La Province in February–March are on-field burning of b) cassava root and c) corn and bushes. d) Large-scale geographical characterization of the Son La site, including the three regions of Indochina, South China Sea and South China denoting distinct BB source regions, corresponding to air mass trajectory analysis sectors.

nutrients to the soil and control weeds and pests. Moreover, traditional stoves were used in most residential homes for indoor or outdoor cooking.

Near-source sampling was performed on fields during typical agricultural residue burning and near cooking places. On the field, crop residues (e.g., cassava root and corn/bushes) were burned, as shown in Figs. 1(b) and 1(c). Wood logs (obtained from local forests) were used for indoor cooking in a traditional stove, and Dimocarpus longan wood was burned in outdoor stoves as well as in outdoor fires. In addition, Dimocarpus longan leaves were burned in a garden. All near-source smoke particles were collected on quartz fiber filters by a MiniVol sampler equipped with a $PM_{2.5}$ size-selective inlet. An overview of the near-source emission samples is presented in Table 1.

In addition to characterization of biomass burning sources from the area surrounding the station the long-range transport from the wider regions of SE Asia, where extensive biomass burning for agricultural practices is known to take place, was examined by means of air mass back trajectories. Back trajectories at starting heights of 300, 500 and 1000 meters a.s.l. were calculated 3 times a day for every 24-hour sampling period. It was assumed that transport within the continental boundary layer would be the most influential on observed concentrations. The HYbrid Single-Particle Lagrangian Integrated Trajectory (HYSPLIT) model (Draxler and Rolph, 2013) was used for the calculations.

Bulk Analyses

OC and EC in the PM_1, $PM_{1–2.5}$, and $PM_{2.5–10}$ samples were determined by the thermal-optical transmittance (TOT) method using a Sunset carbon analyzer (Lab OC-EC Aerosol Analyzer, Sunset Laboratory, Inc.). A NIOSH-like thermal protocol (NIOSH, 1999), with a maximum temperature of 840°C in the He-mode, was applied. $PM_{1–2.5}$ and $PM_{2.5–10}$ aerosol fractions were collected in 60 and 42 spots, respectively, due to the geometry of the corresponding impaction stages of the Dekati impactor. Punches to be analyzed were cut in a carefully designed manner so that the laser beam employed for charring correction illuminated one or more of the sample spots and a quantitative signal change was observed in every thermogram. In addition to EC and OC, carbonate carbon (CC) was determined by manual integration of the sharp peak occurring during the transition to the maximum temperature step in the inert mode (Karanasiou *et al.*, 2011). The detection limit of the instrument was 0.2 μg C cm^{-2}. For $PM_{2.5}$ source emissions samples, OC and EC measurements were performed by using the TOR IMPROVE_A thermal/optical protocol (Chow *et al.*, 2004).

Inorganic cations and anions were measured for PM_1 by ion chromatography (IC) with conductivity detection, using a Dionex ICS-3000 system (Thermo Scientific) (Zhang *et al.*, 2013), while only water-soluble potassium ion data are discussed here. Filter samples were extracted in deionized ultra-pure water by ultrasonic agitation for one hour, followed by filtration through syringe filters. The cation separation was achieved by using a Dionex IonPac CS12 column with a 20 mM methanesulfonic acid eluent at a flow rate of 1.0 mL m^{-1}. The analytical uncertainty for potassium ions was better than 5%, while the detection limit was 2 ng m^{-3}.

In case of the BB source emissions, the inorganic anions and cations were measured by capillary electrophoresis (CE) with UV detection (Kaniansky *et al.*, 1999), using a Capel 103 system (Lumex, Russia). One-fourth filter samples were extracted in 5 mL distillated water by ultrasonic agitation for 45 min, followed by filtration of the extract solutions. The electrolyte for cation measurements contained a mixture of benzimidazole, tartaric acid, and 18-crown-6-ether. Anions were analyzed using chromate buffer consisting of a solution of chromium oxide (VI), diethanolamine, and cetyltrimethylammonium hydroxide.

Water-soluble organic carbon (WSOC) was determined in the aqueous extracts (as describe for IC analysis with additional 1/10 dilution), using a total organic carbon (TOC) analyzer (OI Analytical) based on persulfate oxidation methodology and subsequent detection of the generated CO_2 by a non-dispersive infrared (NDIR) detector.

Quantification of individual polar organic compounds (levoglucosan and mannosan) was carried out by high-performance anion-exchange chromatography (HPAEC), using a Dionex ICS-3000 system (Zhang *et al.*, 2013). Filter portions were extracted in 2 mL ultrapure water in an ultrasonic bath for 60 minutes. The detection limits for levoglucosan and mannosan were 0.4 ng m^{-3} and 0.2 ng m^{-3}, respectively, while the measurement uncertainty was 10%.

The $PM_{2.5}$, $PM_{1–2.5}$, and $PM_{2.5–10}$ samples were also analyzed by Fourier Transform Infrared spectroscopy (FTIR) spectroscopy, in order to determine the functional groups of organic and inorganic compounds. A Shimadzu IRPrestige-21 spectrometer was used in the diffuse reflectance mode. Spectra were measured at 4 cm^{-1} resolution in the

Table 1. Carbon fractions (OC, EC) and ion concentrations (in μg m^{-3}), OC/EC ratios, and levoglucosan (Lev) to mannosan (Man) ratios in smoke released during on-field burning and cooking emissions.

	OC	EC	OC/EC	Lev/Man	Mg^{2+}	Ca^{2+}	SO_4^{2-}	NO_3^-	PO_4^{3-}	Na^+	$HCOO^-$	CH_3COO^-
On-field burning												
cassava root	3802	195	19.5	15.5	107	51.3	23.4	7		65.1		181
corn and bushes	166	28	5.9	17.4	29.6	104	63.7	36	66		12.7	427
longan leaves	1030	52	19.7	11.3	2.8	3.1	7.9	5.2	6.2			145
Cooking												
wood indoors	901	73	12.3	14.3	2.3	1	8.6	4.9			30	559
wood outdoor stove	825	203	4.1	13.5	7.3	32.6	28	12.8	4.5	49.8	22.4	508
wood outdoors	850	192	4.4	12.4	7.1	6.4	28.2	10.7	4.3	14		220

wavenumber range from 4000 to 500 cm^{-1}. In case of $PM_{2.5}$ samples collected on Teflon filters, spectral bands with wave numbers less than 1380 cm^{-1} were not considered because of the strong absorption of the filter material itself. To address the possible inhomogeneity of the sample loading, spectra were collected from five different spots of each sample. If four out of five spectra demonstrated the same absorption bands, we considered these bands as the representative spectrum for the entire sample.

IR Solution software was applied to subtract the FTIR spectrum of oiled blank substrates, to correct the baseline absorbance as well as to perform the Kubelka Munk (KM) conversion of the reflectance spectrum into one which is proportional to the sample concentration (Deb and Verma, 2010). Identification of absorption bands was carried out according to the Shimadzu FTIR database and Coates' practical approach (Coates and Reffner, 2000), as well as using authentic chemical standards. The absorption areas of the most prominent and frequently appearing functional groups were determined in $PM_{1–2.5}$ and $PM_{2.5–10}$ size fractions of 15 samples collected by the Dekati impactor, and in the $PM_{2.5}$ size fraction of 30 samples collected by the MiniVol sampler. Assuming that the chemical compounds providing each functional group do not change markedly from day to day, the relative concentrations of functionalities can be inferred from their relative absorbance areas (Laurent and Allen, 2004). Each functional group absorbance area per m^3 of air sampled in a given day was normalized by the total absorbance area per m^3 of this group taken for all samples collected during the measurement campaign in each size fraction separately. Thus, the relative concentration of each functionality was determined during the entire sampling period.

Individual Particle Analysis

Source and ambient samples were examined using a LEO 1430-vp (Karl Zeiss) field emission scanning electron microscope (SEM) with a spatial resolution of 7 nm, equipped with an Oxford energy dispersive detector (INCA). Energy dispersion X-ray (EDX) spectra for Z elements ($Z \geq 5$) were recorded in SEM image mode. Samples were studied in the high vacuum mode at 10 kV acceleration voltage and a beam current of 1 nA. The detailed procedure was described elsewhere (Bladt *et al.*, 2012; Popovicheva *et al.*, 2012). Briefly, approximately 500–1000 individual particles with a diameter from 0.1 to 1 μm, from 1 to 2.5 μm, and from 2.5 to 10 μm were measured for the PM_1, $PM_{1–2.5}$ and $PM_{2.5–10}$ size fractions, respectively. This number was considered to be sufficient for obtaining a representative overview of groups and types of particles (Liu *et al.*, 2000; Bladt *et al.*, 2012). In the $PM_{2.5}$ samples from on-field burning and cooking emissions the size range of measured particles was from 0.1 to 2.5 μm. Since highly irregular and agglomerated shapes of particles prevent the size distribution to be obtained from SEM images, the averaged size of individual particles was measured using their projected area equivalent diameters.

EDX analysis yielded a data matrix containing C, O, F, Na, Mg, Al, Si, P, S, Cl, K, Ca Ti, and Fe elements at the measured weight concentrations above the detection limit (0.1 wt%). Cluster analysis was applied for separation of individual particles into characteristic groups of similar chemical composition using the software Deductor. Details of the theoretical approach are described elsewhere (Popovicheva *et al.*, 2012). Groups were separated with an average composition as close as possible to physico-chemically identifiable particle types. Naming of particle groups was based on both morphological features and most abundant elements after C and O.

RESULTS AND DISCUSSION

Source Emissions Characterization

Concentrations of OC and EC, as well as OC/EC ratios in on-field and cooking emissions from wood log, cassava root, and leave burning are presented in Table 1. Numerous biomass burning studies show the typical OC/EC for combustion emissions of various biomass species, which depend not only on fuel type but especially also on burning conditions (Reid *et al.*, 2005). On days with substantial smoke impact in Moscow during August 2010, we observed high OC/EC ratios with an average value of 27, comparable with that observed for smoldering burns of regional biomass (Popovicheva *et al.*, 2014a). Fundamental studies in a combustion chamber under controlled conditions provide an effective way for assessing the range of OC/EC ratios specific for each combustion phase (Popovicheva *et al.*, 2015). Elemental carbon particles from Siberian biomass flaming fires comprised a high fraction in total carbon, represented in low OC/EC ratio near 0.5. On the other hand, smoldering fires produced exclusively organic particles with high OC/EC ratios in the range from 34 to 194 (Popovicheva *et al.*, 2015). Thus, small OC/EC ratios around unity are indicative for flaming phase combustion, while higher values are characteristic for smoldering burns. The OC/EC ratios found for on-field and cooking emissions around 4.0 and 19 indicate little open flaming and mixed combustion with significant impact of the smoldering phase, respectively, in accordance with visual observations. Various individual organic compounds, including molecular tracers for biomass burning (i.e., the anhydrosugars levoglucosan and mannosan), were quantified in the source emissions. The relative abundance of levoglucosan (Lev) and mannosan (Man), expressed as the Lev/Man ratio, has been used to indicate specific types of biomass subjected to burning (Engling *et al.*, 2009; Fabbri *et al.*, 2009). The Lev/Man ratios in the smoke particles derived from the field burns and cooking were in the range from 11 to 18 (Table 1), providing a fingerprint for these specific locally used biomass species.

FTIR spectroscopy provides the relative abundance of functional groups representing various organic compounds in the entire aerosol composition. Fig. 2(a) shows the FTIR spectra of particles in the size fraction less than 2.5 μm in on-field and cooking emissions. The prominent absorption bands are related to aliphatic C-C-H (2922–2850 cm^{-1}), acid carbonyl C(O)OH, non-acid carbonyl C=O (1660–1800 cm^{-1}) and carboxylate carbonyl RC(O)O (1650–1580 cm^{-1}) groups. Non-acid carbonyls in ketone- and aldehyde-containing compounds are typically emitted as breakdown

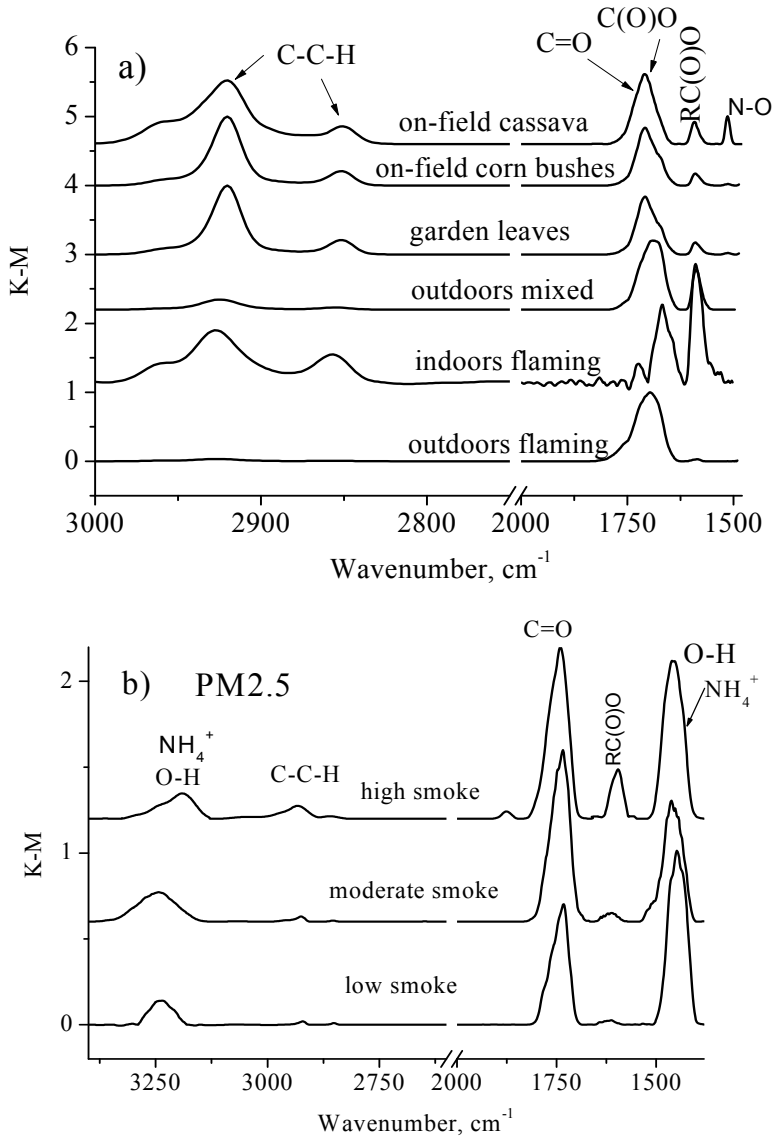

Fig. 2. FTIR spectra of $PM_{2.5}$ size fraction in a) cooking and on-field burning emissions, and b) ambient aerosols. Absorption bands are indicated.

products of lignin during combustion (Simoneit *et al.*, 1993). Carboxylate carbonyls are associated with the most hygroscopic functionality of $RCOO^-$ ions in carboxylic acids and their salts. The dominant abundance of carboxylate ions in these source emissions is confirmed by ion measurements, demonstrating relatively high concentrations of acetate (CH_3COO^-) ions in comparison with inorganic ions such as SO_4^{2-}, NO_3^-, PO_4^{3-}, Na^+, Ca^{2+}, and Mg^{2+} (Table 1). Asymmetric N–O stretches in nitro compounds (near 1514 cm^{-1}) as well as hydroxyl C-OH (3100–3600 cm^{-1}) groups (not shown in Fig. 2(a) can be noted as specific features of on-field smoldering emission.

From cluster analysis of individual particle composition and combined morphological information, groups of particles according to smoke microstructure were obtained for cooking and on-field burning $PM_{2.5}$ emissions (Fig. 3). In wood log smoke released from stove combustion during typical indoor cooking practices, the particles containing mainly C and O with negligible amounts of other elements (< 3 wt%) are assigned to Group *Organic/Soot.* The abundance of this group was found to be as high as 90.5%, being a feature of biomass combustion with small mineral impurities in the biomass (Popovicheva *et al.*, 2015). Some particles in this group show liquid-like amorphous morphology of organic aerosols (Fig. 4.1), forming due to gas-particle condensation of volatile compounds evolved during low-temperature smoldering (Reid *et al.*, 2005). The other particles in this group are soot particles encapsulated with organic species (Fig. 4.2), also observed in emissions from small-scale flaming wood combustion (Osan *et al.*, 2002). Thus, the morphology of cooking-emitted particles indicates both phases of combustion during typical domestic practices. In on-field emissions from burning cassava roots, the abundance of Group *Organic* was found to be near 58%. Besides typical amorphous organic particles, we observed perfect spherical particles (Fig. 4.3), termed “tar balls”

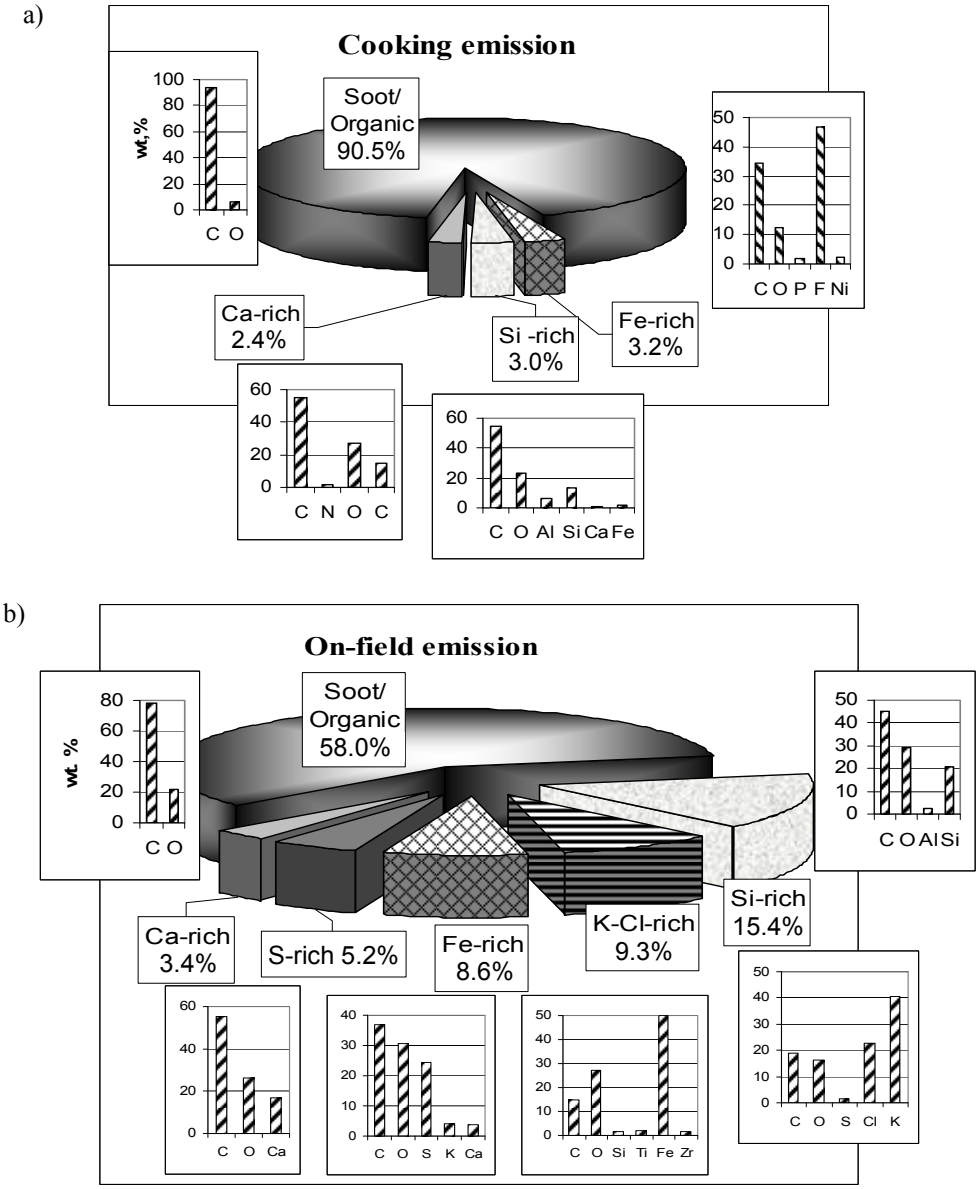

Fig. 3. Grouping of particles from a) stove cooking and b) on-field cassava root burning emissions. Naming, relative abundance, and averaged weight percentage of elements in each group are indicated.

(Hand *et al.*, 2005). Tar balls are believed to be formed due to bimolecular homogeneous nucleation of organic matter with water vapor in the smoldering phase during biomass combustion.

Trace elements in biomass such as Ca, Si, Mg, Al, S, Fe, K, P, Cl, Na, Mn, and Ti are typically also found in BB smoke (Reid *et al.*, 2005). They produce the Group *Ca, Si,* and *Fe-rich* in irregularly shaped particles, where Ca, Si, and Fe are the most abundant elements after C (Fig. 3). In cooking emission, fly ash groups comprise less than 10% of all particles, where calcium oxide, silicon, and iron oxides are predominant (Figs. 4.4, 4.5, and 4.6). A small amount of soil particles was also found in Group *Si and Fe-rich* of aluminosilicates. In on-field burning emissions, Group *Si and Fe-rich* was significantly increased due to appearance of various aluminosilicates such as kaolinite $Al_2Si_3O_5(OH)_4$, K- and Fe-aluminosilicates. This may be due to impact of soil particles suspended by hot convection during combustion of fuels in contact with the ground (Kavouras *et al.*, 2012), because fire produces an upward gas flow through the soil layer, entraining clay, quartz, and other minerals (Samsonov *et al.*, 2012). Moreover, in on-field burning emissions we found Group *S-* and *K,Cl-rich* which is frequently observed in mixed fires (Liu *et al.*, 2000; Osan *et al.*, 2002; Popovicheva *et al.*, 2015). These species are generated due to condensation of sulfates and potassium chlorides after volatile inorganic compounds are vaporized and smoke has cooled. Approximately half of Group *S-rich* contained only S, C and O, indicating that sulfuric acid condensed on carbonaceous particles, while the other half of these particles was composed of potassium and calcium sulfates (Fig. 4.7). Two thirds of the particles in

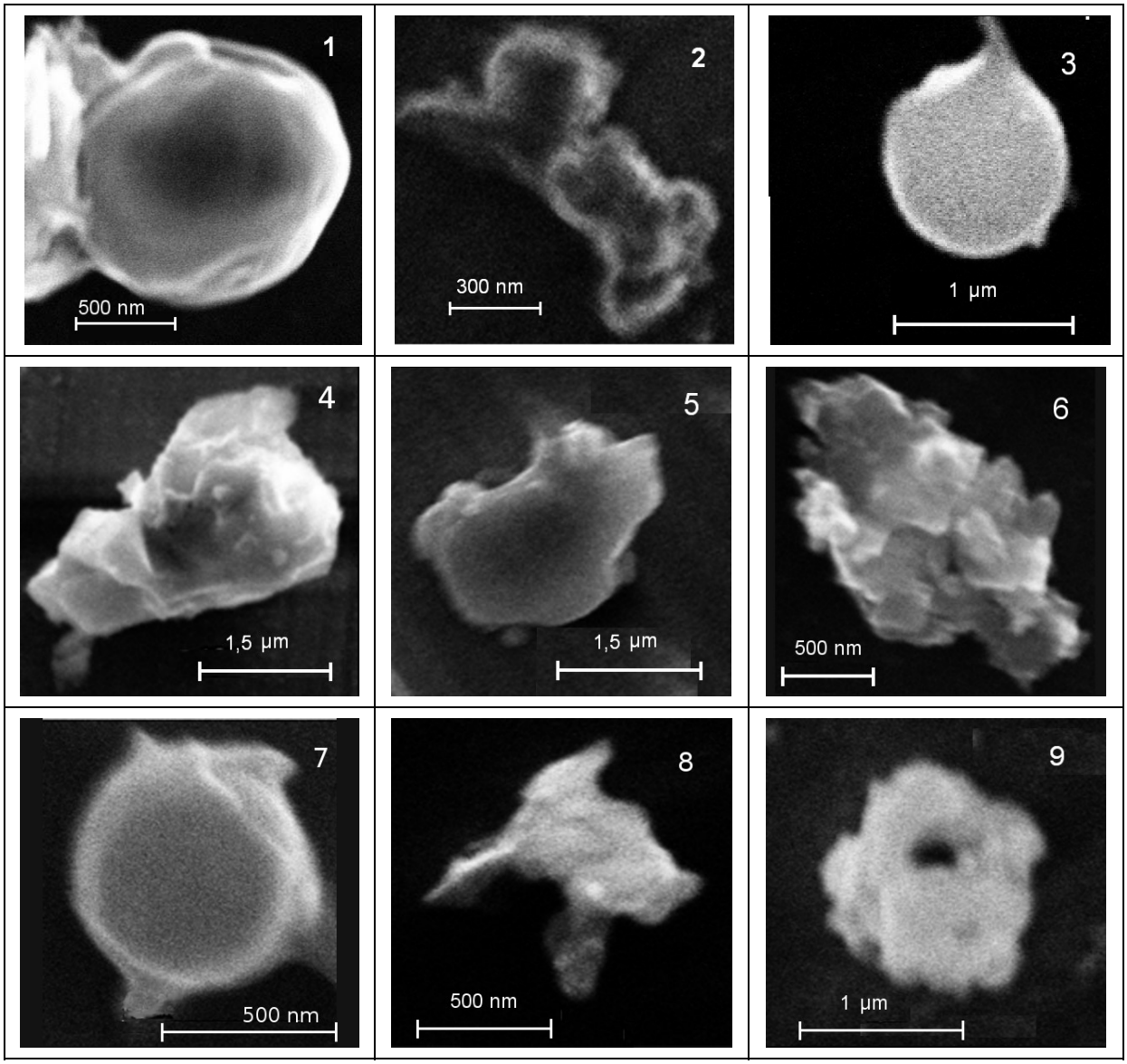

Fig. 4. Representative micrographs of particles from cooking and on-field burning emissions. In Group Soot/Organic 1) organic particle, 2) soot particles encapsulated with organic species, and 3) tar ball; in Group Ca, Si, and Fe-rich 4) calcium oxide, 5) silicon oxide, and 6) iron oxide; in Group S-rich 7) sulfates on carbonaceous particle, 8) potassium sulfate; and in Group K,Cl-rich 9) potassium chloride crystallohydrates.

Group *K,Cl-rich* were potassium chloride crystallohydrates which do not contain C (Fig. 4.9), while the others are KCl salts immersed in the carbonaceous matrix (Fig. 4.8).

PM Evolution and Aerosol Composition during BB Period

Combustion emissions in SE Asia typically peak in spring when the most intense biomass burning activity occurs. A typical view from the Son La measurement site is shown in Fig. 1(a). Evolution of $PM_{2.5}$ mass concentrations at the Son La site during February – April is shown in Fig. 5. As high PM mass concentrations are typically related to BB in this region (Huang *et al.*, 2013; Tsay *et al.*, 2013), the entire 2013 spring measurement campaign could be considered as a BB period. The $PM_{2.5}$ mass concentrations exceeded the WHO (World Health Organization) 24h guideline value of 25 μg m^{-3} on 41 of the total 44 measurement days during the study period, indicating the measured PM levels to be substantially impacted by BB activities. The average $PM_{2.5}$ concentration in Son La was comparable with that (51 ± 32 μg m^{-3}) previously reported in the dry season for a rural site at Tamdao, north of Hanoi (Co *et al.*, 2014).

$PM_{2.5}$ mass concentrations ranged from relatively low values of 40 to high values in excess of 80 μg m^{-3}, associated with smoke of low to high intensity, as shown in Fig. 5.

When the air mass origin of the aerosol observed at Son La is taken into account, the levels of $PM_{2.5}$ mass and carbonaceous particles in the fine fraction can be better understood. According to the air mass residence time in the extended region of SE Asia the aerosol origin is categorized

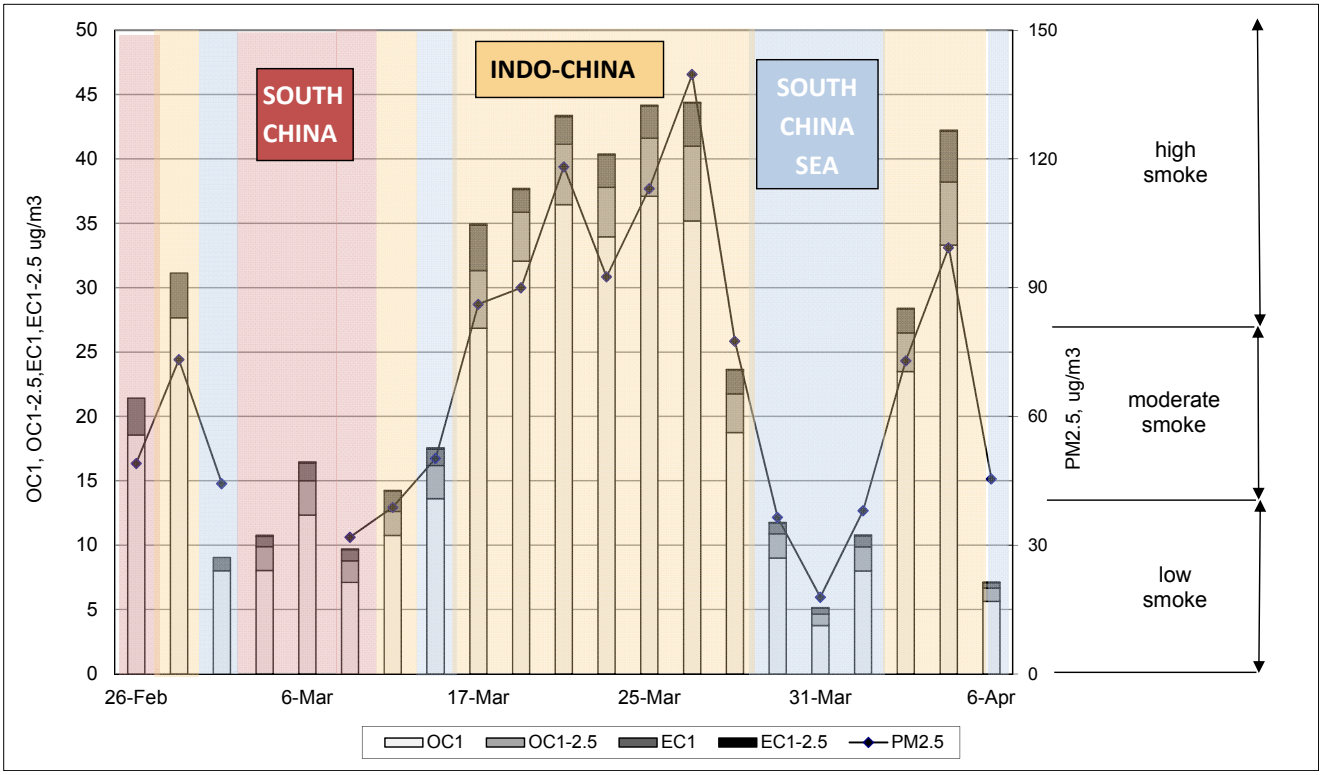

Fig. 5. Concentrations of $PM_{2.5}$ mass, OC_1, $OC_{1–2.5}$, and EC_1 in PM_1 and $PM_{1–2.5}$ during the entire sampling period. The levels of smoke intensity are indicated according to $PM_{2.5}$ mass concentrations.

into three meaningful geographic areas, as shown in Fig. 1(e): South China, where apart from BB other sources such as industry may be active, the area of Indochina where extensive BB occurs and the South China Sea region, where minimum anthropogenic impact is expected. The periods where the major influence is traced to those three areas are marked with different colors in Fig. 5. We can conclude that the Indochina region can as a whole be responsible for an increase in the $PM_{2.5}$ and carbonaceous aerosol fractions by as much as a factor of 3, while the influence from South China was moderate. Background (with respect to biomass burning) concentrations of observed aerosols can be ascribed to times when the air mass origin was from the South China Sea, because it is a marine region. Concentrations at the Son La site are still higher than the WHO limit and are considered to represent the local or regional burden influenced by sources in the surrounding valleys.

The proposed parametrization of the PM mass concentrations is supported by the evolution of aerosol constituents in relation to smoke intensity. Fig. 5 shows OC mass concentrations in PM_1 (OC_1) which are well correlated with smoke evolution, comprising around 30% of $PM_{2.5}$. This finding is in good agreement with the typical carbonaceous nature of BB emissions, showing a clear dominance of OC mass fractions (up to 50%) specifically from smoldering burns (e.g., Alves *et al.*, 2010). Particularly in controlled small-scale fires with limited environmental and soil impacts, OC may approach 67% of PM mass due to condensation of volatilized organics in the smoldering phase (McMeeking *et al.*, 2009). The EC fraction in PM_1 (EC_1) during the BB season was found to be low in comparison with OC_1, yet it correlated well with total $PM_{2.5}$ mass concentrations (Fig. 5). As large EC fractions are typically associated with the flaming phase, low EC1 levels indicate smoldering phase combustion to be dominant during the entire measurement period, characterized by agricultural and domestic burning activities in Son La Province.

Numerous laboratory combustion studies, simulating small-scale fires, have demonstrated carbonaceous particles to be emitted predominantly in the submicron particle range (Hedberg *et al.*, 2002; Wardoyo *et al.*, 2007; Levin *et al.*, 2010). Ambient measurements also revealed the dominance of fine aerosols affected by wildfires with high concentrations of OC and EC (Herckes *et al.*, 2006; Amiridis *et al.*, 2012). In our study the coarser OC fractions, i.e., those in $PM_{1–2.5}$ ($OC_{1–2.5}$) and $PM_{2.5–10}$ ($OC_{2.5–10}$), were found to be much lower than OC_1 during the majority of high smoke days, demonstrating that the carbonaceous particles are almost entirely present in the fine particle fraction during the BB period.

OC/EC ratios are widely used to describe the impact of BB on aerosol chemistry (Reid *et al.*, 2005). Typically, ratios of OC/EC between 4 and 33 are associated with wildfires according to studies conducted in different regions across the globe (Reid *et al.*, 2005; Jaffe *et al.*, 2008), with higher values being associated with smoldering combustion. We found average OC/EC ratios in PM_1 to be 7.6 on days of low smoke and up to 18.3 during high smoke periods (Fig. 6), indicating that smoldering fires were predominant during the dry season in Son La Province. Interestingly, in $PM_{1–2.5}$

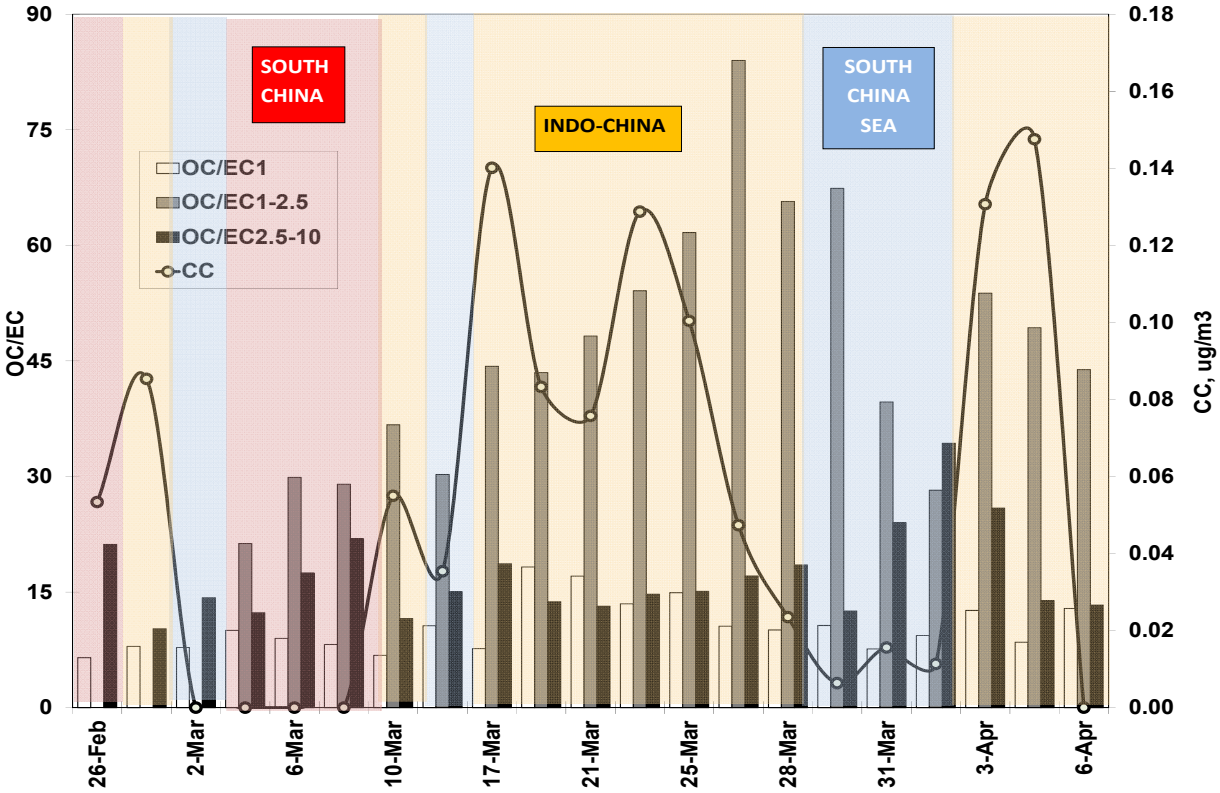

Fig. 6. OC/EC ratios in PM_1 (OC/EC_1), $PM_{1–2.5}$ ($OC/EC_{1–2.5}$), and $PM_{2.5–10}$ ($OC/EC_{2.5–10}$), and carbonate carbon (CC) concentrations in $PM_{2.5–10}$.

and $PM_{2.5–10}$ the OC/EC ratios were even higher than in fine particles (Fig. 6). This may be the consequence of additional OC production from oxidation of fire-produced precursor gases in the atmosphere, leading to the formation of secondary organic aerosols (SOA) (Blando and Turpin, 2000; Engling *et al.*, 2006), along with contributions from biogenic emissions, such as fungal spores (Zhang *et al.*, 2010; Yang *et al.*, 2012).

In Fig. 6 the air mass origin is again highlighted with respect to the evolution of OC/EC ratios and carbonate levels. The most intense episodes with higher concentrations coinciding with transport from Indochina display the most extreme values of OC/EC ratios. Another interesting finding is the appearance of carbonates only during these events of high smoke, presumably related to large-scale agricultural fires from the wider region. This is in agreement with recent findings (Diapouli *et al.*, 2014), when long-range transported smoke from large-scale fires included carbonate salts due to strong thermal convection.

Water-soluble organic carbon (WSOC) concentrations are often used as indicator for photochemical oxidation of OC, leading to SOA formation, while a portion of WSOC can be of primary nature as well, as various oxygenated organic compounds are released directly into the atmosphere from biogenic sources and biomass burning activities. Ambient WSOC concentrations measured in PM_1 (Fig. 7) during this study constituted a substantial fraction (81% on average) of OC. The significant presence of polar organic species is also reflected in the high correlation ($R^2 = 0.88$) between WSOC and OC concentrations, with important implications for climate forcing via the indirect aerosol effect.

Parametrization of smoke intensity during the BB period is useful for quantification of functional groups in ambient aerosols collected during days of similar smoke levels. Representative FTIR spectra are shown in Figs. 2(b) and 8. The prominent absorption bands of acid and non-acid carbonyls, carboxylates, and aliphatic carbon during the whole BB period are similar to those in the on-field and cooking emissions (Fig. 2(a)). Non-acidic carbonyls in addition to carboxylic acid groups were previously found in forest fire emissions and were assigned to aldehyde/ketone, ester/lactone, and acid anhydride groups (Russell *et al.*, 2009). A band of aliphatic carbon in low smoke periods may be a feature of the urban background, because alkanes dominate functionalities of diesel emissions (Popovicheva *et al.*, 2014b). The band of ammonium NH^+ (3350–3100 cm^{-1}) is prominent in ambient aerosols.

The absorption areas per m^3 of air sampled for the individual functional groups were determined for each day. The relative concentrations for each functional group, normalized based on the total absorbance area per m^3 during the whole BB period, are shown in Fig. 9 for $PM_{2.5}$, $PM_{1–2.5}$, and $PM_{2.5–10}$ size fractions. In $PM_{2.5}$ all organic functionalities increase throughout the study period, correlating well with the smoke levels and OC evolution. Conversely, the relative concentrations of ammonium are not well correlated with the smoke intensity, indicating regional source influence other than from BB.

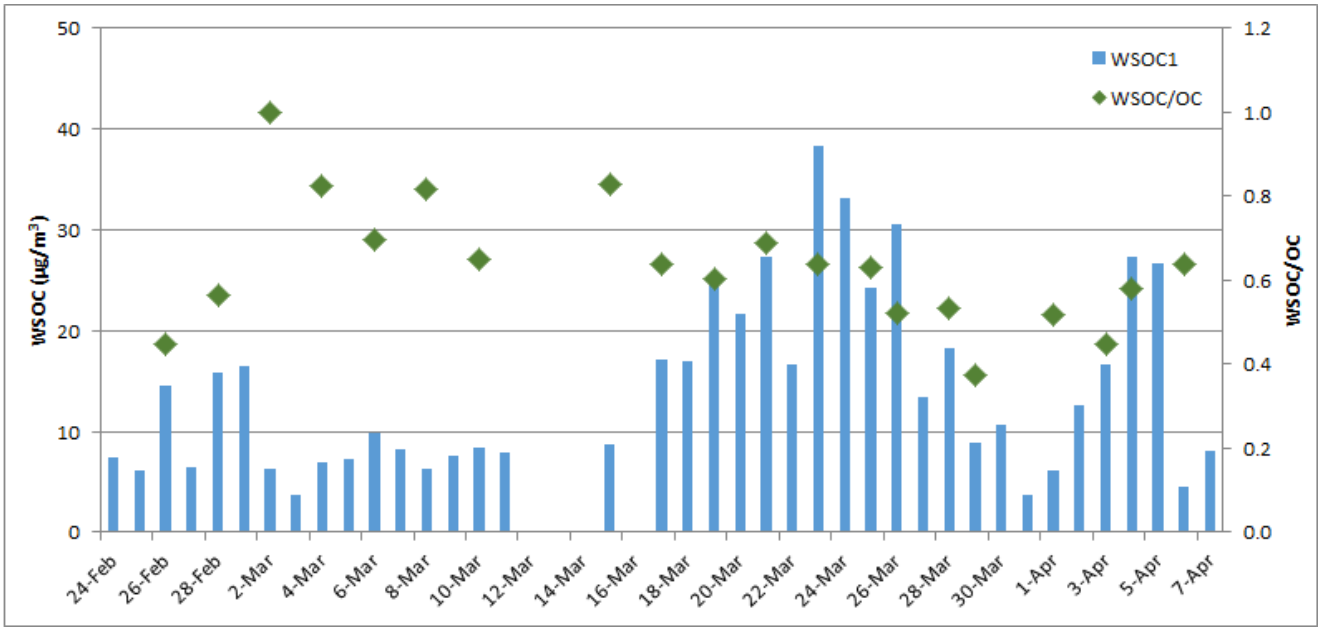

Fig. 7. Concentration timeline of water-soluble organic carbon (WSOC) in PM_1 size fraction, as well as WSOC/OC fractions.

Organic functionalities in coarse particles were prominent in both size fractions (Fig. 8), while their relative concentrations are not well correlated with the smoke levels (Fig. 9). Since the $PM_{2.5}$ size fraction includes particles in the range from 1 to 2.5 μm, we conclude that the organic compounds of smoke origin can be for the most part categorized as submicron particles, according to the largest OC concentrations measured in PM_1. Organic compounds in supermicron particles may have additional sources such as SOA and microbial activities, as mentioned above. The other prominent bands of C-N-H in amines (near 1550 cm^{-1}) on days of low smoke can be assigned to biogenic functional groups (Coury and Dillner, 2009), and were consequently absent in high smoke periods.

Dust functionalities are specific features of coarse particles. Fig. 8 shows the prominent band of silicate ions (SiO_4^{4-}) in various aluminosilicates with the variable position near 1000 cm^{-1}. Carbonates (CO_3^{2-}) were identified in the range 880–860 cm^{-1}, and their presence in the $PM_{2.5-10}$ size fraction was confirmed by TOT measurements of carbonates in form of carbonate carbon (CC, Fig. 6). Relative concentrations of carbonates are increasing from low to high smoke (Fig. 9), correlating well with the OC evolution (Fig. 6), thus showing the impact of re-suspended soil particles during intensive agricultural fires on the composition of coarse ambient aerosols.

The SO_4^{2-} absorption band (580–700 cm^{-1}) was well identified together with those of NH_4^+ in coarse particles (Fig. 8). The lack of correlation with the smoke levels indicates the predominance of regional sources for sulfates and ammonium, in addition to emissions from local industry. As reported by Huang *et al.* (2013), only 30–40% of the sulfur deposition in Vietnam originates from domestic sources, with the rest contributed mainly by southern China and Thailand.

Enhancement of the ambient concentrations of BB tracers (levoglucosan and K^+ ion) by two orders of magnitude indicates strong influence from BB emissions resulting in a regional smoke haze episode. The BB tracer size distributions are characterized by a unimodal pattern peaking in the particle size range of 0.4–1.0 μm (Zhang *et al.*, 2015). For ambient aerosol during the BB period we found that the levoglucosan and K^+ ion concentrations in PM_1 correlated well with each other (R^2 = 0.91) and with $PM_{2.5}$ mass evolution (Fig. 10), supporting the smoke parametrization during the entire BB period. The ambient concentrations of the two BB tracers (levoglucosan and K^+) in PM_1 were in the range of 0.19 to 2.79 μg m^{-3} and 0.20 to 2.00 μg m^{-3}, respectively, with average values of 1.22 and 0.95 μg m^{-3}. The relative contributions of levoglucosan and K^+ to PM_1 mass were 2.2% and 1.7%, respectively, similar to previous observations between 0.5% and 6% of PM depending on biomass type (Reid *et al.*, 2005; Alves *et al.*, 2010). An average K^+/EC ratio of 0.2 obtained during the high smoke period was between the values for smoldering and flaming fires obtained during a recent regional-scale biomass burning episode (Popovicheva *et al.*, 2014a), and in good agreement with values reported from previous biomass burning studies (Andreae, 1983).

An additional molecular BB tracer, mannosan (derived from the thermal decomposition of hemicellulose), showed the same temporal pattern as levoglucosan, as evidenced in the high correlation (R^2 = 0.98) between the ambient concentrations of the two tracers. Moreover, the relative abundance of these two anhydrosugars (expressed in form of the Lev/Man ratio) can be used as indicator of the biomass type that produced the smoke particles. Based on Lev/Man ratios from previously reported source emission studies and the results from the near-source measurements of locally average Lev/Man ratio of 14.6 in PM_1 indicates a mix of

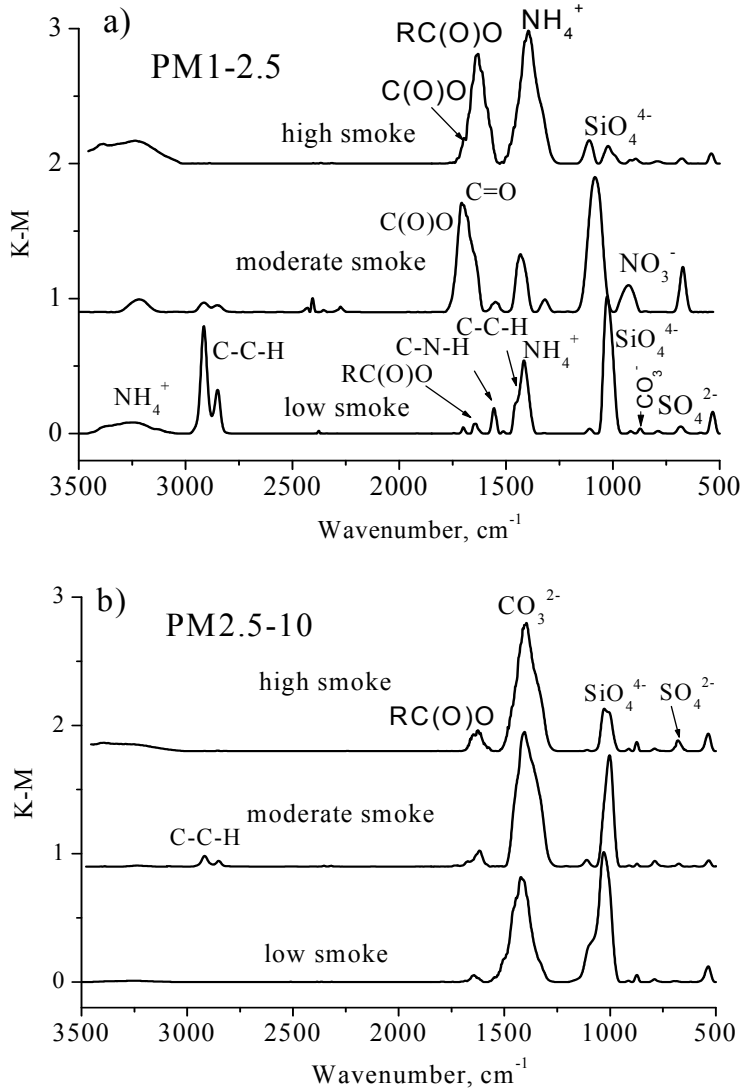

Fig. 8. FTIR spectra of coarse particles in a) $PM_{1–2.5}$, and b) $PM_{2.5–10}$ size fraction of ambient aerosols.

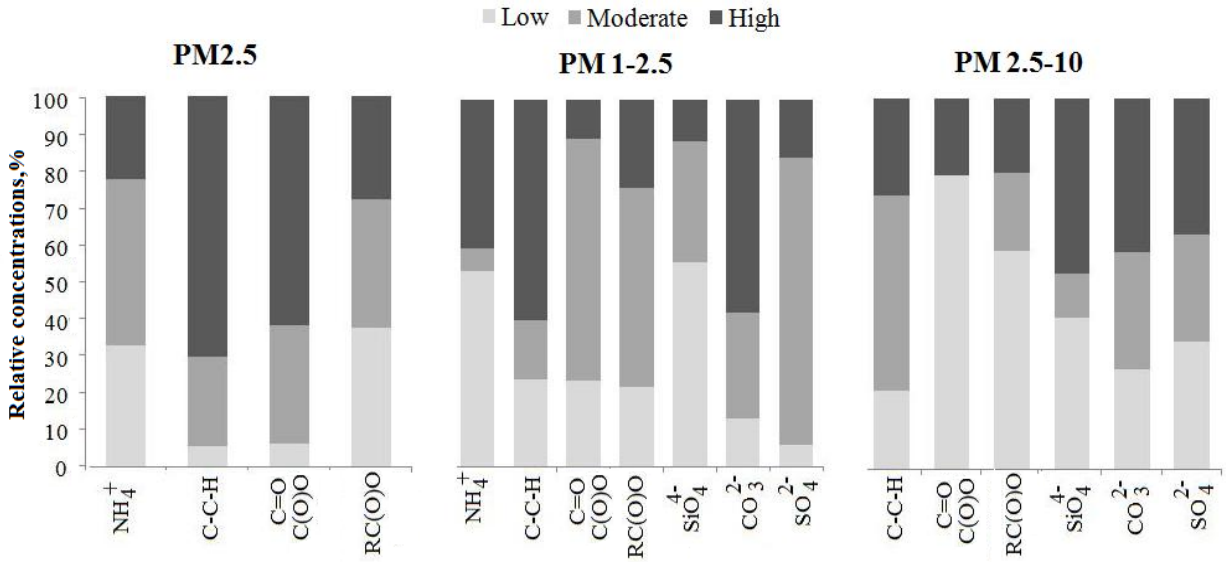

Fig. 9. Relative concentrations of NH_4^+, aliphatic C-C-H, carbonyl C=O and C(O)O, carboxylate RC(O)O, CO_3^-, and SO_4^{2-} in $PM_{2.5}$, $PM_{1–2.5}$, and $PM_{2.5–10}$ size fractions during low, moderate, and high smoke periods.

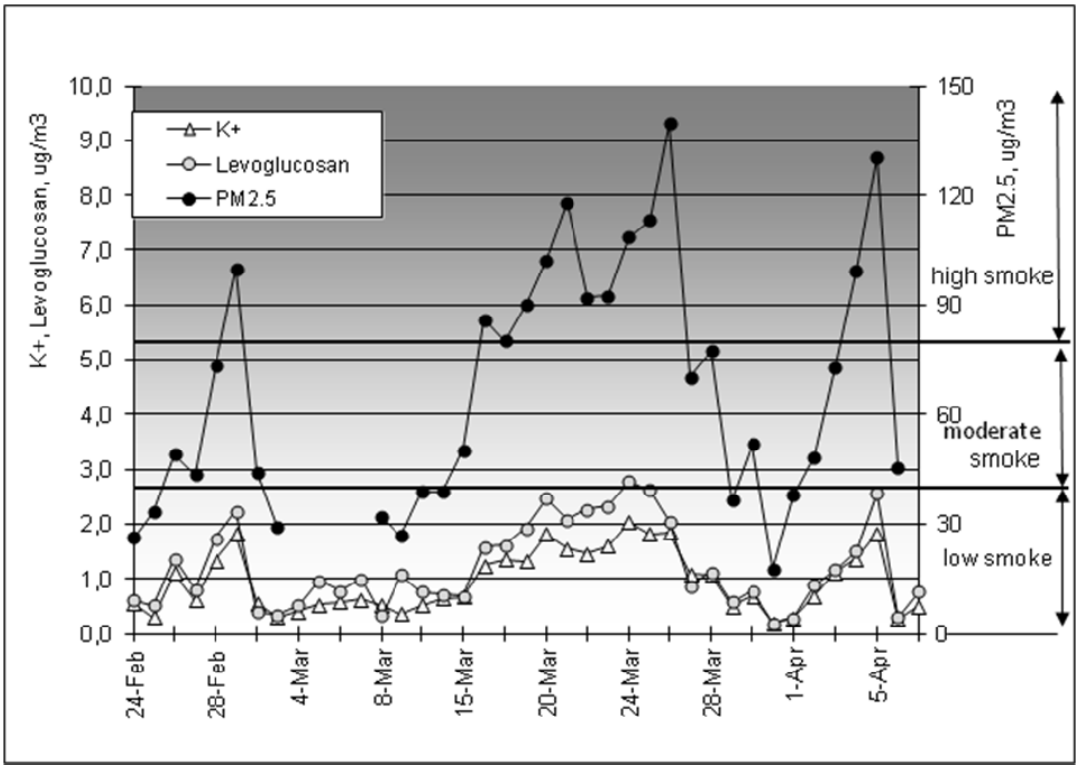

Fig. 10. Concentrations of $PM_{2.5}$ mass, K^+, and levoglucosan in PM_1 throughout the sampling period.

burned species in Son La Province (see section 3.1), the hard wood and grasses/straw with minor contributions from softwood burning as the sources for the sampled BB aerosol. Overall, the significant impact of BB emissions on fine aerosol during the study period was demonstrated by the strong correlation between ambient PM_1 levels of levoglucosan and OC as well as WSOC (R^2 = 0.94 and 0.84, respectively).

Smoke Microstructure

Morphology and Elemental Composition

Ambient aerosols collected during the BB period in Son La Province exhibited a large variability of sizes and morphological types, including spherical, chain, and crystalline mineral particles. Organic particles were frequently found in roughly spherical or liquid-like shape, while soot can be clearly distinguished by chain agglomerates of ultrafine primary particles. Fly ash and dust were observed with solid irregular shapes of round and euhedral morphology similar to those particles found in on-field and cooking source emissions.

Fig. 11(a) shows the elemental composition of individual particles collected on days of similar smoke levels for each PM size, showing consistent carbonaceous character, i.e., particles containing mainly C and O. In fine particles (PM_1) the C content increased with smoke intensity from 30 to 80%, clearly demonstrating BB as a major source of elevated PM concentrations. On the other hand, the O abundance decreased from 42 to 18% between low and high smoke periods, indicating that particles were more oxidized in low smoke periods than the relatively fresher smoke particles observed during high smoke days, likely due to the abundance of local biomass burning emissions. Only Si and S impacted the mass of fine aerosols (besides C and O), at 5 and 10 wt%, respectively. However, in coarse particles ($PM_{1–2.5}$ and $PM_{2.5–10}$ size fractions) trace elements such as Mg, Al, Ca, and Fe, as well as Si and S, comprised 1 to 10% of the total PM mass, representing fly ash and dust.

Individual particle analyses showed the highly heterogeneous distribution of elements over particles in the size-segregated ambient aerosols (Fig. 11(b)). In the PM_1 fraction Mg, Al, Si, Ca, S, and K were found to be the most frequently distributed elements after C and O, which were even more abundant in low smoke periods. In contrast, in the $PM_{1–2.5}$ and $PM_{2.5–10}$ fractions the opposite pattern was observed: smoke impacted mostly the coarse particles by an increased abundance of these trace elements. This finding was prominent for sulfur content which was influenced by other sources different from local biomass combustion, as discussed above.

Grouping of Size-Segregated Aerosols

Based on composition and morphology analysis, distinct types of aerosols such as soot, tar balls, and organic particles with inorganic inclusions dominated by potassium and sulfates were previously identified in fire emissions (Posfai *et al.*, 2003; Hand *et al.*, 2005). Our SEM/EDX analyses show carbonaceous particles internally/externally mixed with inorganic fly ash and dust comprising smoke-influenced aerosol during the BB period in Son La Province. Groups of particles obtained by cluster analyses are presented for low, moderate, and high smoke in Fig. 12.

In low smoke periods, Group *S-rich* was found to be most abundant in the fine fraction, accounting for 62.1% of PM_1 particle number. Around 44% of this group was composed of sulfates condensed on carbonaceous particles due to coagulation and heterogeneous nucleation. 20% of Group *S-rich* were sulfates mixed with K, Ca, Mg - aluminosilicates, while the remaining part were Ca, Mg, and K - containing salts. The representative micrographs of this group are shown in Fig. 13. In coarse fractions the types of sulfates are the same but one of the sulfate salts condensed on carbonaceous particles is half as abundant.

Group *Si-rich* is next in respect to abundance after *S-rich* in low smoke, clearly demonstrating dust impact. Especially in the $PM_{2.5–10}$ fraction *Si-rich* particles approach 43.4% and are composed of various K, Ca, Mg, Fe-aluminosilicates of soil origin (Fig. 13). In the fine PM_1 fraction this group is also mixed with sulfur.

The abundance of Group *Soot/Organic* is consistently

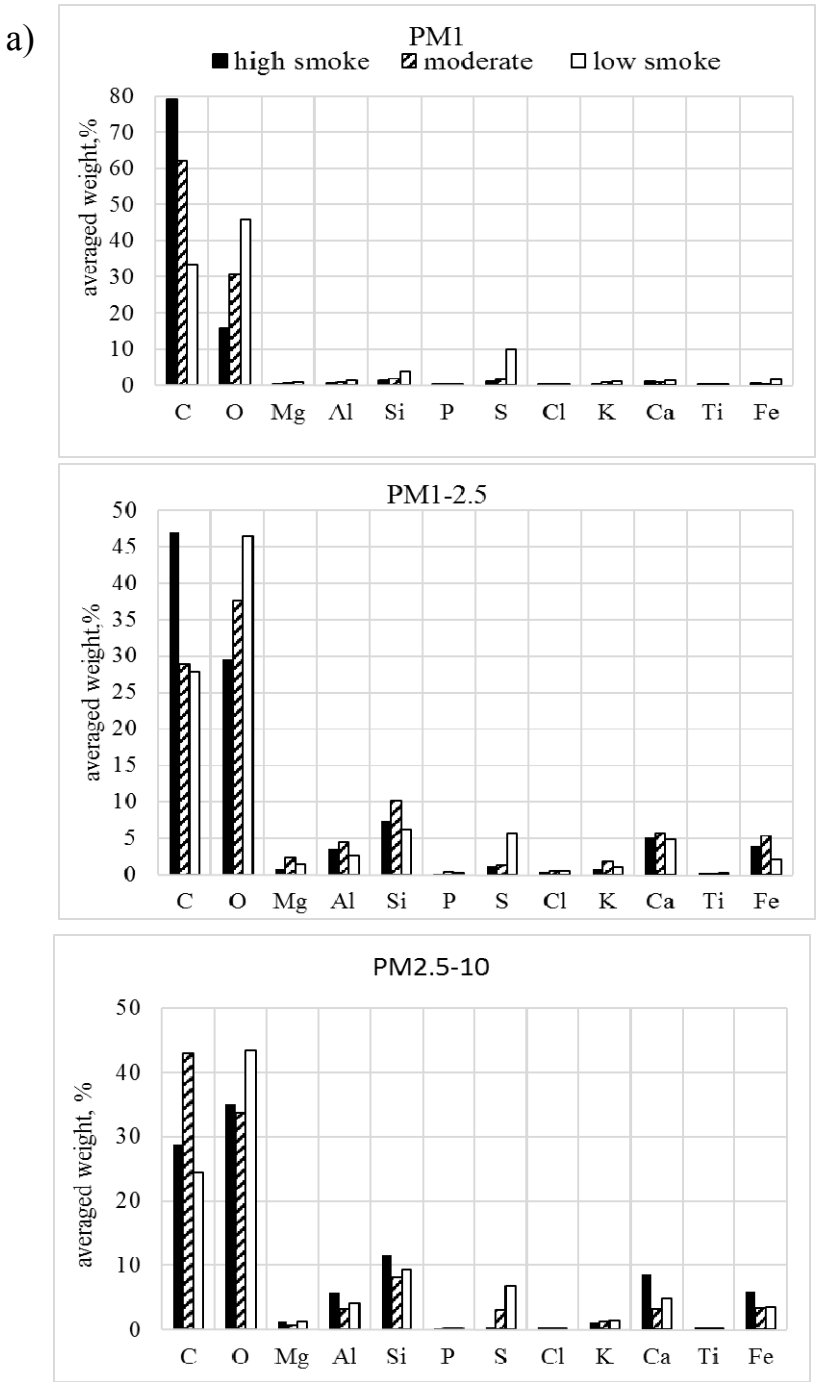

Fig. 11. a) Averaged weight percentages of elements and b) abundance of elements over particles during low, moderate, and high smoke periods of PM_1, $PM_{1–2.5}$ and $PM_{2.5–10}$ size fractions. Elements with an abundance of less than 2%, such as Na and F, are not shown.

b)

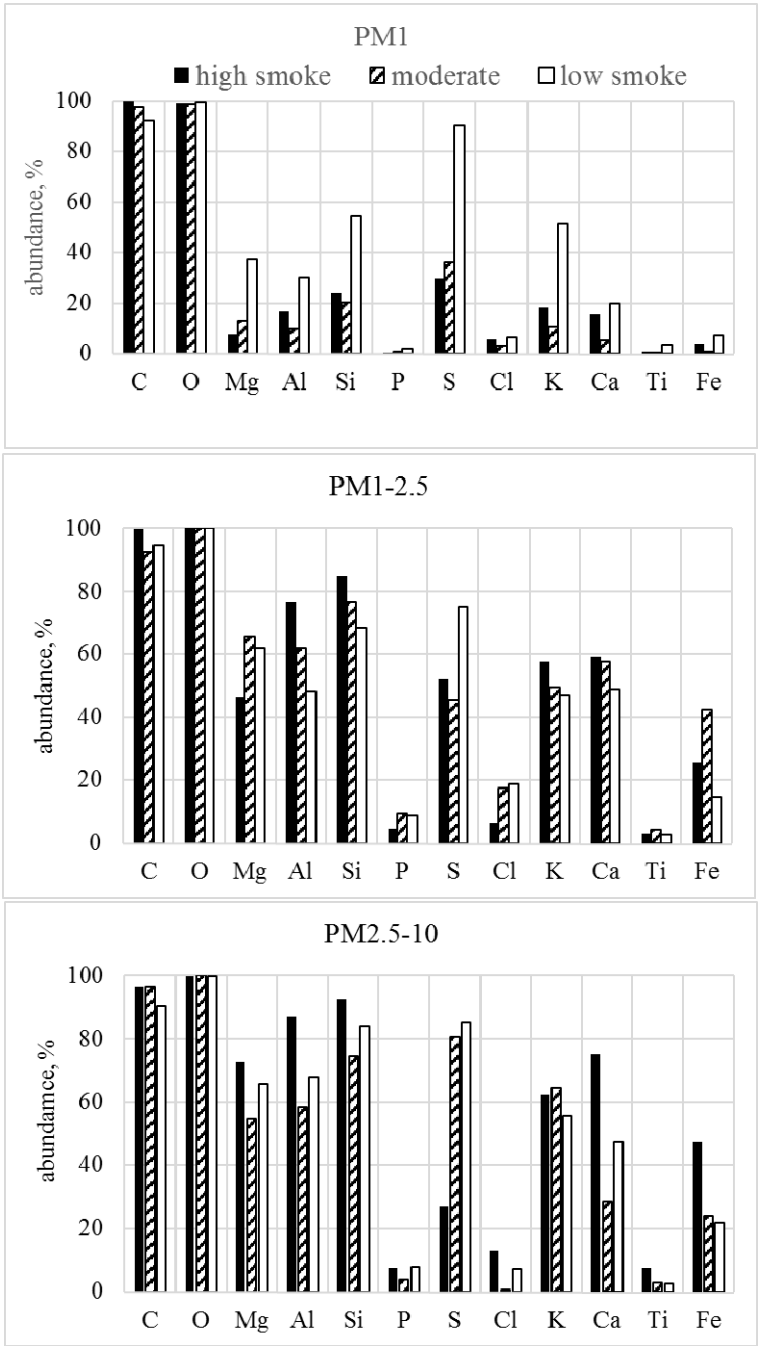

Fig. 11. (*continued*).

higher in the fine particle microstructure than in coarse particles. During days of low smoke only 12% of aerosols have the morphology and composition of soot and organic particles, which roughly resembles background conditions. In urban environments of megacities approximately 17% of all ambient particles were found to belong to Group *Soot/Organic*, being mainly of traffic origin (Diapouli *et al.*, 2014; Popovicheva *et al.*, 2014b). Representative micrographs of the soot agglomerates in Fig. 13 depict diesel engine emissions from Son La city. Groups with Ca and Fe being predominant after C and O, containing calcium oxides, sulfates, and Ca-aluminosilicates as well as iron sulfates and Fe-aluminosilicates, were less abundant. The smallest Group *Na and Mg-rich* with chloride/sulfates were found during days of low smoke.

With increasing smoke intensity, the abundance of Group *Soot/Organic* was strongly enlarged to 59% and 68% in moderate and high smoke, respectively. Soot agglomerates were observed in the hazy atmosphere of Son La, indicating flaming phase smoke emissions. However, shapeless organic particles and spherical tar balls were found more frequently (Fig. 13) as a morphological feature of particles generated during smoldering combustion in the surroundings of the Son La measurement station, also well in accordance

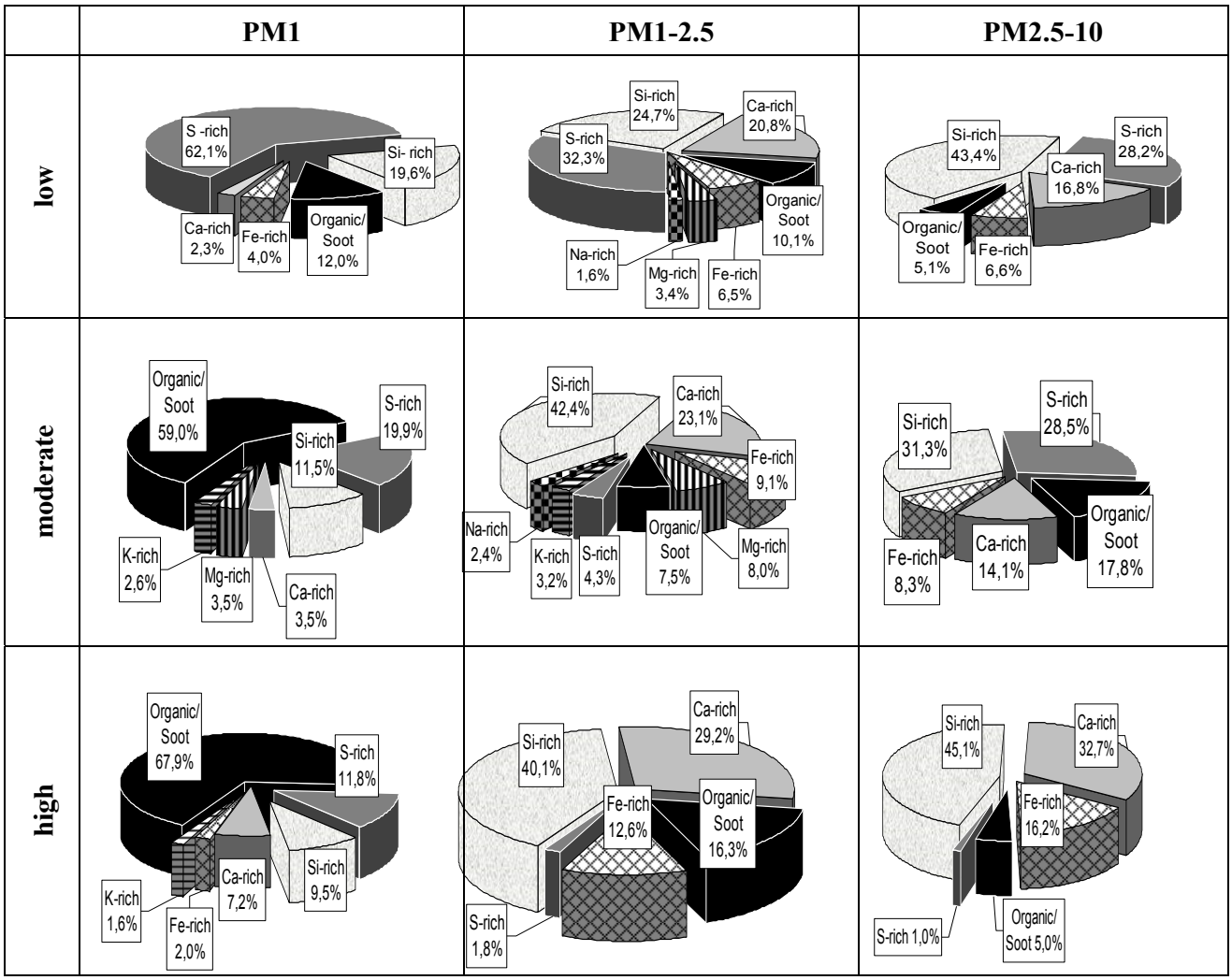

Fig. 12. Groups of particles obtained by cluster analyses for low, moderate, and high smoke in three size fractions.

with higher OC/EC ratio produced by smoldering. Therefore, we may propose that submicrometer amorphous carbon spheres of tar balls, ubiquitously observed in Asian outflow with spectral absorption features of brown carbon (Alexander *et al.*, 2008), may originate from intensive burning practices in SE Asia, such as those during dry seasons in Vietnam, as observed in this study.

With increasing smoke intensity, the abundance of Group *S-rich* was significantly decreased to 11.8%. Group *K-rich* appeared in moderate and high smoke in the PM_1 fraction, where K is either condensed on carbonaceous particles or generated externally mixed potassium sulfates and chlorides (Fig. 13). Since potassium in ionic form (K^+), acting as a BB tracer, demonstrated good correlation with the smoke intensity (Fig. 8), we may consider Group *K-rich* as marker of smoke microstructure during periods of intensive fires.

The larger the particle size, the smaller was the abundance of Group *Soot/Organic* on days of high smoke (Fig. 13), accounting for 67% in PM_1, 16.3% in $PM_{1–2.5}$, and 5% in $PM_{2.5–10}$ of all particles in each size fraction. On the other hand, the other mineral groups of fly ash and soil origin, Groups *Ca and Si-rich*, were most abundant in the coarse mode. Group *Ca-rich* was composed of calcium sulfates, Ca-aluminosilicates, and particles almost entirely comprised of C, Ca, and O, which could be in form of calcium carbonates, in accordance with CO_3^{2-} functionalities and carbonate carbon (CC), as mentioned above. The last conclusion can be supported by the fact that Triassic soils in the Son La region contain lime (CaO), dolomite ($CaMg(CO_3)_2$), limestone ($CaCO_3$, in calcite and aragonite), and marlstone ($CaCO_3$) with variable amounts of clays and silt (Nam, 1995; Stahr *et al.*, 2010; Oo *et al.*, 2013; Stahr *et al.*, 2013).

CONCLUSIONS

$PM_{2.5}$ mass concentrations were evolved from low to high smoke intensity during the spring time biomass burning season in northwest Vietnam, significantly exceeding the WHO air quality standards. The proposed parameterization of $PM_{2.5}$ mass concentrations with respect to smoke intensity was supported by evolution of aerosol components during the BB period. Comprehensive characterization of bulk

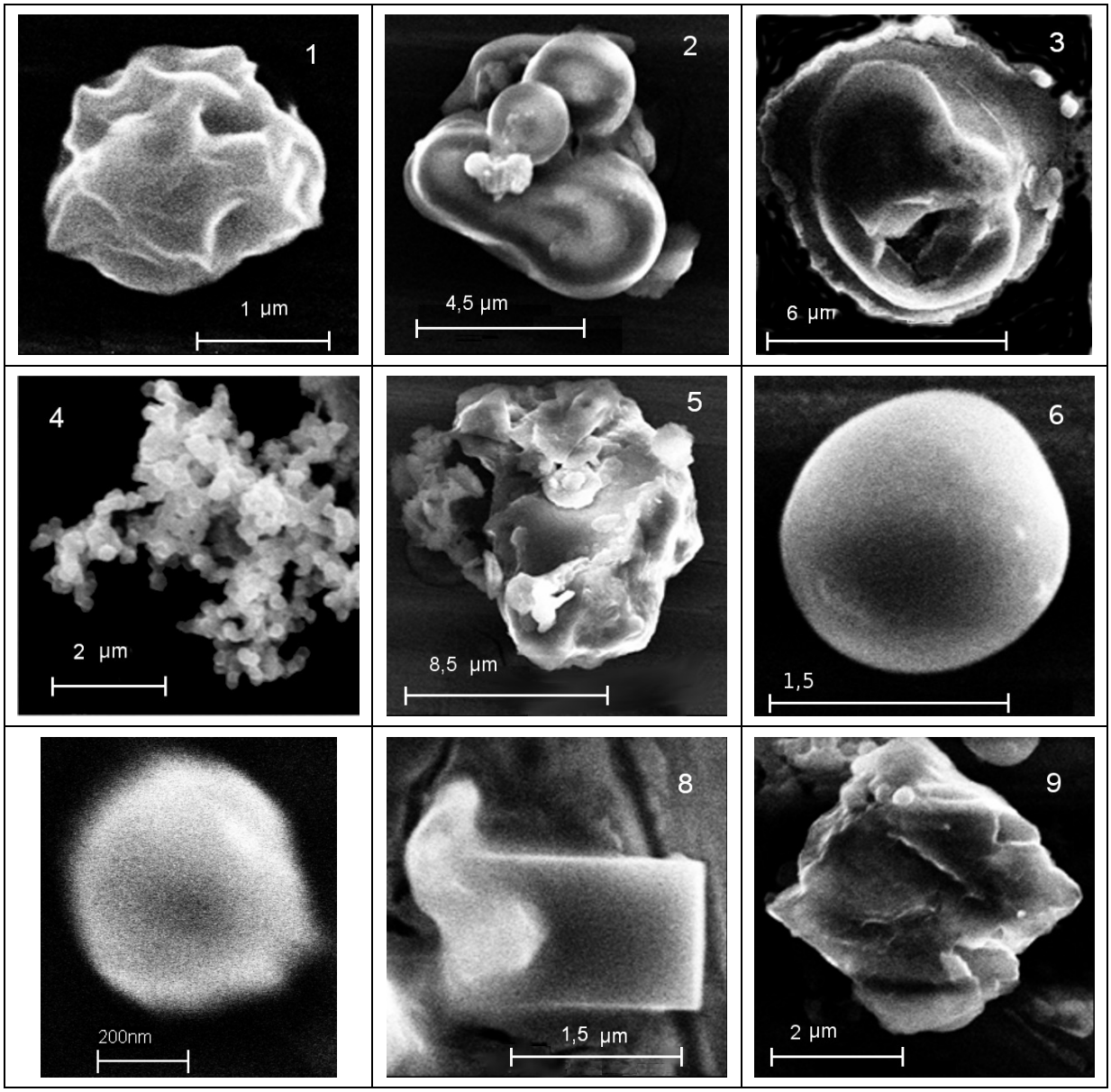

Fig. 13. Representative micrographs of ambient aerosols in low smoke in Group S-rich: 1) predominantly C, O, S; 2) S condensed on K-aluminosilicates; 3) magnesium sulfates, in Group Soot/Organic; 4) soot agglomerates, in Group Si-rich; 5) Mg, Ca, K- aluminosilicates, in high smoke in Group Soot/Organic; 6) tar ball, in Group K-rich; 7) K condensed on organic particles, in Group Ca-rich; 8) calcium/potassium sulfate; 9) calcium carbonate.

aerosol constituents showed the impacts of BB emissions on PM mass and composition. The Indochina region, where extensive BB occurs periodically, is responsible for an increase in the $PM_{2.5}$ and carbonaceous aerosol fractions by as much as a factor of 3, while the influence from South China, where apart from BB other sources such as industry may be active, was moderate. Minimum anthropogenic impact was observed for background concentrations ascribed to times when the air mass origin was from the marine region of the South China Sea.

Measurement of size-segregated OC, EC, anhydrosugars, and inorganic species revealed the main chemical components comprising the ambient aerosols, with the BB constituents found predominantly in submicron particles. Analyses of carbon fractions, organic and inorganic functionalities, and individual particle grouping led to conclusion that ambient aerosols have been highly affected by emissions from the smoldering combustion of wood and other local biomass species. Aerosol chemistry and specifically patterns of three BB tracers (levoglucosan, mannosan and K^+) indicated the dominant impacts of agricultural and domestic combustion sources during the intensive BB period.

Individual particle analyses showed that carbonaceous particles, comprised mainly of polar organic compounds internally/externally mixed with inorganic fly ash and dust, constituted a characteristic multicomponent smoke aerosol amenable for establishing smoke micromarkers in ambient aerosol.

ACKNOWLEDGMENTS

Financial support from MOST 101-2923-M-007-004-MY3, RFBR-NSC 12-05-92002, RFBR-VAST 15-5554020 and VAST. HTQT. NGA. 04/15-16, and the EnTeC FP7 Capacities programme (REGPOT-2012-2013-1, FP7, ID: 316173) is kindly acknowledged.

REFERENCES

Alexander, D.T.L., Crozier, P.A. and Anderson, J.R. (2008). Brown carbon spheres in East Asian outflow and their optical properties. *Science* 321: 833–836.

Alves, C.A., Goncalves, C., Pio, C.A., Mirante, F., Caseiro, A., Tarelho, L., Freitas, M.C. and Viegas, D.X. (2010). Smoke emissions from biomass burning in a Mediterranean shrubland. *Atmos. Environ.* 44: 3024–3033.

Amiridis, V., Zerefos, C., Kazadzis, S., Gerasopoulos, E., Eleftheratos, K., Vrekoussis, M., Stohl, A., Mamouri, R.E., Kokkalis, P., Papayannis, A., Eleftheriadis, K., Diapouli, E., Keramitsoglou, I., Kontoes, C., Kotroni, V., Lagouvardos, K., Marinou, E., Giannakaki, E., Kostopoulou, E., Giannakopoulos, C., Richter, A., Burrows, J.P. and Mihalopoulos, N. (2012). Impact of the 2009 Attica wild fires on the air quality in urban Athens. *Atmos. Environ.* 46: 536–544.

Andreae, M.O. (1983). Soot carbon and excess fine potassium: Long-range transport of combustion-derived aerosols. *Science* 220: 1148–1151.

Andrews, E., Saxena, P., Musarra, S., Hildemann, L.M., Koutrakis, P., McMurry, P.H., Olmez, I. and White, W.H. (2000). Concentration and composition of atmospheric aerosols from the 1995 SEAVS experiment and a review of the closure between chemical and gravimetric measurements. *J. Air Waste Manage. Assoc.* 50: 648–664.

Bladt, H., Schmid, J., Kireeva, E.D., Popovicheva, O.B., Perseantseva, N.M., Timofeev, M.A., Heister, K., Uihlein, J., Ivleva, N.P. and Niessner, R. (2012). Impact of Fe content in laboratory-produced soot aerosol on its composition, structure, and thermo-chemical properties. *Aerosol Sci. Technol.* 46: 1337–1348.

Blando, J.D. and Turpin, B.J. (2000). Secondary organic aerosol formation in cloud and fog droplets: A literature evaluation of plausibility. *Atmos. Environ.* 34: 1623–1632.

Bond, T.C., Doherty, S.J., Fahey, D.W., Forster, P.M., Berntsen, T., DeAngelo, B.J., Flanner, M.G., Ghan, S., Karcher, B., Koch, D., Kinne, S., Kondo, Y., Quinn, P.K., Sarofim, M.C., Schultz, M.G., Schulz, M., Venkataraman, C., Zhang, H., Zhang, S., Bellouin, N., Guttikunda, S.K., Hopke, P.K., Jacobson, M.Z., Kaiser, J.W., Klimont, Z., Lohmann, U., Schwarz, J.P., Shindell, D., Storelvmo, T., Warren, S.G. and Zender, C.S. (2013). Bounding the role of black carbon in the climate system: A scientific assessment. *J. Geophys. Res.* 118: 5380–5552.

Chen, K., Yin, Y., Kong, S.F., Xiao, H., Wu, Y.X., Chen, J.H. and Li, A.H. (2014). Size-resolved chemical composition of atmospheric particles during a straw burning period at Mt. Huang (the Yellow Mountain) of China. *Atmos. Environ.* 84: 380–389.

Chow, J.C., Watson, J.G., Chen, L.W.A., Arnott, W.P., Moosmueller, H. and Fung, K. (2004). Equivalence of elemental carbon by thermal/optical reflectance and transmittance with different temperature protocols. *Environ. Sci. Technol.* 38: 4414–4422.

Chuang, M.T., Chou, C.C.K., Sopajaree, K., Lin, N.H., Wang, J.L., Sheu, G.R., Chang, Y.J. and Lee, C.T. (2013). Characterization of aerosol chemical properties from near-source biomass burning in the northern Indochina during 7-SEAS/Dongsha experiment. *Atmos. Environ.* 78: 72–81.

Co, H.X., Dung, N.T., Oanh, N.T.K., Hang, N.T., Phuc, N.H. and Le, H.A. (2014). Levels and Composition of Ambient Particulate Matter at a Mountainous Rural Site in Northern Vietnam. *Aerosol Air Qual. Res.* 14: 1917–1928

Coates, J. (2000). Interpretation of Infrared Spectra, a Practical Approach. In *Encyclopedia of Analytical Chemistry*, Meyers, R.A. (Ed.), John Wiley and Sons, Chichester, pp. 10815–10837.

Coury, C. and Dillner, A.M. (2009). ATR-FTIR characterization of organic functional groups and inorganic ions in ambient aerosols at a rural site. *Atmos. Environ.* 43: 940–948.

Deb, M.K. and Verma, D. (2010). Fourier transform infrared spectroscopic determination of ammonium at sub-microgram level in waters and biological fluids following removal of nitrate from sample matrix by zerovalent iron nanoparticles. *Microchim. Acta* 169: 23–31.

Diapouli, E., Popovicheva, O., Kistler, M., Vratolis, S., Persiantseva, N., Timofeev, M., Kasper-Giebl, A. and Eleftheriadis, K. (2014). Physicochemical characterization of aged biomass burning aerosol after long-range transport to Greece from large scale wildfires in Russia and surrounding regions, Summer 2010. *Atmos. Environ.* 96: 393–404.

NOAA ARL READY Website (2013). http://www.arl.noaa.gov/HYSPLIT.php.

Engling, G., Herckes, P., Kreidenweis, S.M., Malm, W.C. and Collett Jr, J.L. (2006). Composition of the fine organic aerosol in Yosemite National Park during the 2002 Yosemite Aerosol Characterization Study. *Atmos. Environ.* 40: 2959–2972.

Engling, G., Lee, J.J., Tsai, Y.W., Lung, S.C.C., Chou, C.C.K. and Chan, C.Y. (2009). Size-resolved anhydrosugar composition in smoke aerosol from controlled field burning of rice straw. *Aerosol Sci. Technol.* 43: 662–672.

Engling, G., Zhang, Y.N., Chan, C.Y., Sang, X.F., Lin, M., Ho, K.F., Li, Y.S., Lin, C.Y. and Lee, J.J. (2011). Characterization and sources of aerosol particles over the southeastern Tibetan Plateau during the Southeast Asia biomass-burning season. *Tellus Ser B* 63: 117–128.

Engling, G., He, J., Betha, R. and Balasubramanian, R. (2014). Assessing the regional impact of Indonesian biomass burning emissions based on organic molecular tracers and chemical mass balance modeling. *Atmos. Chem. Phys.* 14: 8043–8054.

Fabbri, D., Torri, C., Simonei, B.R.T., Marynowski, L.,

Rushdi, A.I. and Fabianska, M.J. (2009). Levoglucosan and other cellulose and lignin markers in emissions from burning of Miocene lignites. *Atmos. Environ.* 43: 2286–2295.

Gustafsson, O., Krusa, M., Zencak, Z., Sheesley, R.J., Granat, L., Engstrom, E., Praveen, P.S., Rao, P.S.P., Leck, C. and Rodhe, H. (2009). Brown Clouds over South Asia: Biomass or Fossil Fuel Combustion? *Science* 323: 495–498.

Hand, J.L., Malm, W.C., Laskin, A., Day, D., Lee, T., Wang, C., Carrico, C., Carrillo, J., Cowin, J.P., Collett, J. and Iedema, M.J. (2005). Optical, physical, and chemical properties of tar balls observed during the Yosemite Aerosol Characterization Study. *J. Geophys. Res.* 110: D21210.

Hedberg, E., Kristensson, A., Ohlsson, M., Johansson, C., Johansson, P., Swietlicki, E., Vesely, V. and Wideqvist, U. (2002). Chemical and physical characterization of emissions from birch wood combustion in a wood stove. *Atmos. Environ.* 36: 4823–4837.

Herckes, P., Engling, G., Kreidenweis, S.M. and Collett, J.L., Jr. (2006). Particle size distributions of organic aerosol constituents during the 2002 Yosemite Aerosol Characterization Study. *Environ. Sci. Technol.* 40: 4554–4562.

Ho, K.F., Engling, G., Ho, S.S.H., Huang, R.J., Lai, S.C., Cao, J.J. and Lee, S.C. (2014). Seasonal variations of anhydrosugars in $PM_{2.5}$ in the Pearl River Delta Region, China. *Tellus Ser B.* 66.

Huang, K., Fu, J.S., Hsu, N.C., Gao, Y., Dong, X.Y., Tsay, S.C. and Lam, Y.F. (2013). Impact assessment of biomass burning on air quality in Southeast and East Asia during BASE-ASIA. *Atmos. Environ.* 78: 291–302.

Jaffe, D., Hafner, W., Chand, D., Westerling, A. and Spracklen, D. (2008). Interannual variations in $PM_{2.5}$ due to wildfires in the Western United States. *Environ. Sci. Technol.* 42: 2812–2818.

Kaniansky, D., Masar, M., Marak, J. and Bodor, R. (1999). Capillary electrophoresis of inorganic anions. *J. Chromatogr. A* 834: 133–178.

Karanasiou, A., Diapouli, E., Cavalli, F., Eleftheriadis, K., Viana, M., Alastuey, A., Querol, X. and Reche, C. (2011). On the quantification of atmospheric carbonate carbon by thermal/optical analysis protocols. *Atmos. Meas. Tech.* 4: 2409–2419.

Kavouras, I.G., Nikolich, G., Etyemezian, V., DuBois, D.W., King, J. and Shafer, D. (2012). In situ observations of soil minerals and organic matter in the early phases of prescribed fires. *J. Geophys. Res.* 117: D12313.

Laurent, J.P. and Allen, D.T. (2004). Size distributions of organic functional groups in ambient aerosol collected in Houston, Texas. *Aerosol Sci. Technol.* 38: 82–91.

Levin, E.J.T., McMeeking, G.R., Carrico, C.M., Mack, L.E., Kreidenweis, S.M., Wold, C.E., Moosmuller, H., Arnott, W.P., Hao, W.M., Collett, J.L. and Malm, W.C. (2010). Biomass burning smoke aerosol properties measured during Fire Laboratory at Missoula Experiments (FLAME). *J. Geophys. Res.* 115: D18210.

Lim, S., Lee, M., Lee, G., Kim, S., Yoon, S. and Kang, K. (2012). Ionic and carbonaceous compositions of PM_{10}, $PM_{2.5}$ and $PM_{1.0}$ at Gosan ABC Superstation and their ratios as source signature. *Atmos. Chem. Phys.* 12: 2007–2024.

Lin, N.H., Tsay, S.C., Maring, H.B., Yen, M.C., Sheu, G.R., Wang, S.H., Chi, K.H., Chuang, M.T., Ou-Yang, C.F., Fu, J.S., Reid, J.S., Lee, C.T., Wang, L.C., Wang, J.L., Hsu, C.N., Sayer, A.M., Holben, B.N., Chu, Y.C., Nguyen, X.A., Sopajaree, K., Chen, S.J., Cheng, M.T., Tsuang, B.J., Tsai, C.J., Peng, C.M., Schnell, R.C., Conway, T., Chang, C.T., Lin, K.S., Tsai, Y.I., Lee, W.J., Chang, S.C., Liu, J.J., Chiang, W.L., Huang, S.J., Lin, T.H. and Liu, G.R. (2013). An overview of regional experiments on biomass burning aerosols and related pollutants in Southeast Asia: From BASE-ASIA and the Dongsha Experiment to 7-SEAS. *Atmos. Environ.* 78: 1–19.

Liu, H.Y., Jacob, D.J., Bey, I., Yantosca, R.M., Duncan, B.N. and Sachse, G.W. (2003). Transport pathways for Asian pollution outflow over the Pacific: Interannual and seasonal variations. *J. Geophys. Res.* 108: 8786.

Liu, X.D., Van Espen, P., Adams, F., Cafmeyer, J. and Maenhaut, W. (2000). Biomass burning in southern Africa: Individual particle characterization of atmospheric aerosols and savanna fire samples. *J. Atmos. Chem.* 36: 135–155.

McMeeking, G.R., Kreidenweis, S.M., Baker, S., Carrico, C.M., Chow, J.C., Collett, J.L., Hao, W.M., Holden, A.S., Kirchstetter, T.W., Malm, W.C., Moosmuller, H., Sullivan, A.P. and Wold, C.E. (2009). Emissions of trace gases and aerosols during the open combustion of biomass in the laboratory. *J. Geophys. Res.* 114: D19210.

Nam, T.N. (1995). The geology of Vietnam: A brief summary and problems. *Geosci. Rep. Shizuoka Univ.* 22: 1–9.

Niemi, J.V., Saarikoski, S., Tervahattu, H., Makela, T., Hillamo, R., Vehkamaki, H., Sogacheva, L. and Kulmala, M. (2006). Changes in background aerosol composition in Finland during polluted and clean periods studied by TEM/EDX individual particle analysis. *Atmos. Chem. Phys.* 6: 5049–5066.

Oo, A.Z., Win, K.T., Nguyen, L. and Kimura, S.D.B. (2013). Toposequential variation in soil properties and crop yield from double-cropping paddy rice in Northwest Vietnam. *J. Cereals Oilseeds* 4: 65–75.

Osan, J., Alfoldy, B., Torok, S. and Van Grieken, R. (2002). Characterisation of wood combustion particles using electron probe microanalysis. *Atmos. Environ.* 36: 2207–2214.

Park, S.S., Sim, S.Y., Bae, M.S. and Schauer, J.J. (2013). Size distribution of water-soluble components in particulate matter emitted from biomass burning. *Atmos. Environ.* 73: 62–72.

Popovicheva, O., Kireeva, E., Persiantseva, N., Timofeev, M., Bladt, H., Ivleva, N.P., Niessner, R. and Moldanova, J. (2012). Microscopic characterization of individual particles from multicomponent ship exhaust. *J. Environ. Monit.* 14: 3101–3110.

Popovicheva, O., Kistler, M., Kireeva, E., Persiantseva, N.,

Timofeev, M., Kopeikin, V. and Kasper-Giebl, A. (2014a). Physicochemical characterization of smoke aerosol during large-scale wildfires: Extreme event of August 2010 in Moscow. *Atmos. Environ.* 96: 405–414.

Popovicheva, O.B., Kireeva, E.D., Steiner, S., Rothen-Rutishauser, B., Persiantseva, N.M., Timofeev, M.A., Shonija, N.K., Comte, P. and Czerwinski, J. (2014b). Microstructure and chemical composition of diesel and biodiesel particle exhaust. *Aerosol Air Qual. Res.* 14: 1392–1401.

Popovicheva, O.B., Kozlov, V.S., Engling, G., Diapouli, E., Persiantseva, N.M., Timofeev, M.A., Fan, T.S., Saraga, D. and Eleftheriadis, K. (2015). Small-scale study of siberian biomass burning: I. smoke microstructure. *Aerosol Air Qual. Res.* 15: 117–128.

Posfai, M., Simonics, R., Li, J., Hobbs, P.V. and Buseck, P.R. (2003). Individual aerosol particles from biomass burning in southern Africa: 1. Compositions and size distributions of carbonaceous particles. *J. Geophys. Res.* 108: 8483.

Ramanathan, V., Crutzen, P.J., Kiehl, J.T. and Rosenfeld, D. (2001). Atmosphere - Aerosols, climate, and the hydrological cycle. *Science* 294: 2119–2124.

Reid, J.S., Koppmann, R., Eck, T.F. and Eleuterio, D.P. (2005). A review of biomass burning emissions part II: intensive physical properties of biomass burning particles. *Atmos. Chem. Phys.* 5: 799–825.

Russell, L.M., Takahama, S., Liu, S., Hawkins, L.N., Covert, D.S., Quinn, P.K. and Bates, T.S. (2009). Oxygenated fraction and mass of organic aerosol from direct emission and atmospheric processing measured on the R/V Ronald Brown during TEXAQS/GoMACCS 2006. *J. Geophys. Res.* 114: D00F05.

Samsonov, Y.N., Ivanov, V.A., McRae, D.J. and Baker, S.P. (2012). Chemical and dispersal characteristics of particulate emissions from forest fires in Siberia. *Int. J. Wildland Fire* 21: 818–827.

Simoneit, B.R.T., Rogge, W.F., Mazurek, M.A., Standley, L.J., Hildemann, L.M. and Cass, G.R. (1993). Lignin pyrolysis products, lignans, and resin acids as specific tracers of plant classes in emissions from biomass combustion. *Environ. Sci. Technol.* 27: 2533–2541.

Simoneit, B.R.T., Schauer, J.J., Nolte, C.G., Oros, D.R., Elias, V.O., Fraser, M.P., Rogge, W.F. and Cass, G.R. (1999). Levoglucosan, a tracer for cellulose in biomass burning and atmospheric particles. *Atmos. Environ.* 33: 173–182.

Stahr, K., Schuler, U., Haring, V., Clemens, G., Herrmann, L. and Zarei, M. (2010). Clay and Oxide Mineralogy of Different Limestone Soils in Southeast Asia. Proccedings of World Congress of Soil Science, Soil Solutions for a Changing World, pp. 37–39.

Stahr, K., Clemens, G., Schuler, U., Erbe, P., Haering, V., Cong, N.D., Bock, M., Tuan, V.D., Hagel, H. and Le Vinh, B. (2013). *Beyond the Horizons: Challenges and Prospects for Soil Science and Soil Care in Southeast Asia*, Sustainable Land Use and Rural Development in Southeast Asia: Innovations and Policies for Mountainous Areas, Springer, pp. 31–107.

Tao, J., Zhang, L.M., Engling, G., Zhang, R.J., Yang, Y.H., Cao, J.J., Zhu, C.S., Wang, Q.Y. and Luo, L. (2013). Chemical composition of $PM_{2.5}$ in an urban environment in Chengdu, China: Importance of springtime dust storms and biomass burning. *Atmos. Res.* 122: 270–283.

Tsay, S.C., Hsu, N.C., Lau, W.K.M., Li, C., Gabriel, P.M., Ji, Q., Holben, B.N., Welton, E.J., Nguyen, A.X., Janjai, S., Lin, N.H., Reid, J.S., Boonjawat, J., Howell, S.G., Huebert, B.J., Fu, J.S., Hansen, R.A., Sayer, A.M., Gautam, R., Wang, S.H., Goodloe, C.S., Miko, L.R., Shu, P.K., Loftus, A.M., Huang, J., Kim, J.Y., Jeong, M.J. and Pantina, P. (2013). From BASE-ASIA toward 7-SEAS: A satellite-surface perspective of boreal spring biomass-burning aerosols and clouds in Southeast Asia. *Atmos. Environ.* 78: 20–34.

Wardoyo, A.Y.P., Morawska, L., Ristovski, Z.D., Jamriska, M., Carr, S. and Johnson, G. (2007). Size distribution of particles emitted from grass fires in the Northern Territory, Australia. *Atmos. Environ.* 41: 8609–8619.

Xie, R.K., Seip, H.M., Leinum, J.R., Winje, T. and Xiao, J.S. (2005). Chemical characterization of individual particles (PM_{10}) from ambient air in Guiyang City, China. *Sci. Total Environ.* 343: 261–272.

Yang, Y.H., Chan, C.Y., Tao, J., Lin, M., Engling, G., Zhang, Z.S., Zhang, T. and Su, L. (2012). Observation of elevated fungal tracers due to biomass burning in the Sichuan Basin at Chengdu City, China. *Sci. Total Environ.* 431: 68–77.

Zhang, T., Engling, G., Chan, C.Y., Zhang, Y.N., Zhang, Z.S., Lin, M., Sang, X.F., Li, Y.D. and Li, Y.S. (2010). Contribution of fungal spores to particulate matter in a tropical rainforest. *Environ. Res. Lett.* 5: 024010.

Zhang, Y.N., Zhang, Z.S., Chan, C.Y., Engling, G., Sang, X.F., Shi, S. and Wang, X.M. (2012). Levoglucosan and carbonaceous species in the background aerosol of coastal southeast China: Case study on transport of biomass burning smoke from the Philippines. *Environ. Sci. Pollut. Res.* 19: 244–255.

Zhang, Z., Gao, J., Engling, G., Tao, J., Chai, F., Zhang, L., Zhang, R., Sang, X., Chan, C.Y., Lin, Z. and Cao, J. (2015). Characteristics and applications of size-segregated biomass burning tracers in China's Pearl River Delta region. *Atmos. Environ.* 102: 290–301.

Zhang, Z.S., Engling, G., Chan, C.Y., Yang, Y.H., Lin, M., Shi, S., He, J., Li, Y.D. and Wang, X.M. (2013). Determination of isoprene-derived secondary organic aerosol tracers (2-methyltetrols) by HPAEC-PAD: Results from size-resolved aerosols in a tropical rainforest. *Atmos. Environ.* 70: 468–476.

Received for review, November 22, 2015
Revised, May 8, 2016
Accepted, June 18, 2016